






Iron Reduction Controls Carbon Mineralization in Aquaculture Shrimp Pond Sediments in Subtropical Estuaries

Ji Tan^{1,2,3,4} , Min Luo^{2,4} , Fengfeng Tan^{1,2,3}, Eric Lichtfouse⁵ , Changwei Zhang^{1,2,4}, Xin Chen^{1,2,4} , Jiafang Huang^{1,2,3} , Yang Tan⁶, and Leilei Xiao^{6,7}

¹Key Laboratory of Humid Subtropical Eco-Geographical Process, Ministry of Education, Fujian Normal University, Fuzhou, China, ²Research Center of Geography and Ecological Environment, Fuzhou University, Fuzhou, China, ³College of Geography Science, Fujian Normal University, Fuzhou, China, ⁴College of Environment and Safety Engineering, Fuzhou University, Fuzhou, China, ⁵Aix-Marseille University, CNRS, IRD, INRAE, CEREGE, Aix en Provence, France, ⁶CAS Key Laboratory of Coastal Environmental Processes and Ecological Remediation, Yantai Institute of Coastal Zone Research, Chinese Academy of Sciences, Yantai, China, ⁷Shandong Key Laboratory of Coastal Environmental Processes, Yantai, China

Key Points:

- Aquaculture farming activities enhance microbial Fe(III) reduction rates
- High-salinity ponds have lower rates of microbial Fe(III) reduction than low-salinity ponds
- Microbial Fe(III) reduction plays a significant role in carbon mineralization in sediments of aquaculture shrimp ponds

Supporting Information:

Supporting Information may be found in the online version of this article.

Correspondence to:

M. Luo and L. Xiao,
luomin@fzu.edu.cn;
llxiao@yic.ac.cn

Citation:

Tan, J., Luo, M., Tan, F., Lichtfouse, E., Zhang, C., Chen, X., et al. (2022). Iron reduction controls carbon mineralization in aquaculture shrimp pond sediments in subtropical estuaries. *Journal of Geophysical Research: Biogeosciences*, 127, e2022JG007081. <https://doi.org/10.1029/2022JG007081>

Received 20 JUL 2022

Accepted 1 DEC 2022

Author Contributions:

Formal analysis: Ji Tan, Fengfeng Tan, Changwei Zhang, Xin Chen, Yang Tan

Funding acquisition: Min Luo, Leilei Xiao

Investigation: Ji Tan, Fengfeng Tan, Changwei Zhang, Xin Chen, Jiafang Huang

Methodology: Min Luo, Jiafang Huang, Leilei Xiao

Supervision: Min Luo, Leilei Xiao

Writing – original draft: Ji Tan, Min Luo

Writing – review & editing: Min Luo, Eric Lichtfouse, Leilei Xiao

Abstract Expanding worldwide aquaculture has greatly increased greenhouse gas emissions; however, the underlying microbial mechanisms are poorly understood. In particular, the role of ferric iron [Fe(III)] (hydro) oxides in carbon mineralization in aquaculture pond sediments remains unclear. Here, we studied the rates of microbial Fe(III) reduction, sulfate reduction, methanogenesis, and carbon mineralization in aquaculture shrimp (*Litopenaeus vannamei*) ponds of various salinities before, during, and after shrimp farming in subtropical estuaries in southeast China. Sediment samples (0–10 cm) were collected to investigate the content of iron species, characteristics of organic matter, and abundance of *Geobacter*, a proxy of iron reducers. Overall, Fe(III) reduction ($46.1\% \pm 19.1\%$) dominated carbon mineralization, followed by sulfate reduction ($39.6\% \pm 16.8\%$) and methanogenesis ($1.5\% \pm 1.1\%$). Microbial Fe(III) reduction contributed more to carbon mineralization during farming than before and after farming. This enhancement in Fe(III) reduction is attributed to a significant increase in Fe(III) content during farming. Additionally, the contributions of microbial Fe(III) reduction to carbon mineralization were lower in the high-salinity ponds than in the low-salinity ponds due to the suppression of sulfate reduction, abiotic Fe(III) reduction by sulfides, and lower oxidation-reduction potential. Our findings demonstrate that microbial Fe(III) reduction plays a significant role in carbon mineralization in aquaculture pond sediments. Future carbon flux prediction models of aquaculture pond systems should fully integrate microbial Fe(III) reduction.

Plain Language Summary The expanding global aquaculture industry has greatly increased the carbon mineralization potential (i.e., production of carbon dioxide and methane). Carbon mineralization is mediated by various types of microbial respiration, including iron reduction, sulfate reduction, and methanogenesis. Aquatic sediments are enriched with iron oxides; however, the contribution of microbial iron reduction to carbon mineralization in the aquaculture sediments is poorly understood. Here, we studied the rates and pathways of carbon mineralization in aquaculture shrimp (*Litopenaeus vannamei*) ponds of varying salinities before, during, and after shrimp farming in subtropical estuaries in southeast China. Our results show that microbial iron reduction has a larger contribution to carbon mineralization during farming than before and after farming. In addition, the contributions of microbial iron reduction to carbon mineralization were lower in the high-salinity ponds than in the low-salinity ponds. Overall, microbial iron reduction contributed approximately 46% to carbon mineralization, followed by sulfate reduction (approximately 40%) and methanogenesis (approximately 2%). Our findings demonstrate that microbial iron reduction plays a significant role in carbon mineralization in aquaculture pond sediments. Microbial Fe(III) reduction should be involved in future carbon flux prediction models of aquaculture pond systems.

1. Introduction

Global aquaculture production has increased by 500% since the late 1980s to address the growing demand for aquatic proteins and decreasing fishery resources in natural aquatic ecosystems (FAO, 2016). More than 40% of global aquaculture production is carried out in earthen aquaculture ponds (Yuan et al., 2019). A total volume of 101 million tons of aquaculture was produced in 2014, and this volume is expected to continuously increase to 230 million tons in the next 20 years (FAO, 2014). Such huge increases in aquatic production depend heavily on

high stocking densities and large amounts of aquafeed inputs (Naylor et al., 2021). Unfortunately, approximately 35% of aquafeed cannot be utilized by aquatic animals, which leads to large amounts of residual aquafeed or feces accumulating in aquaculture pond sediments (Pereyra et al., 2010). These organic-rich biodeposit stimulate carbon mineralization and yield carbon greenhouse gases such as carbon oxides (CO₂) and methane (CH₄) (Burkholder & Shumway, 2011). It is estimated that the annual CO₂ emissions of aquaculture ponds are equal to 7.1×10^3 CO₂-eq m⁻² (Tong, Bastviken, et al., 2021), which accounts for 15.1% of CO₂ emissions in inland waters (Holgerson & Raymond, 2016). Although much attention has been paid to greenhouse gas emission fluxes from aquaculture ponds (Yang et al., 2018; Yuan et al., 2021, 2019; Zhang et al., 2022), little is known about the mechanisms underlying microbially mediated carbon mineralization, which leads to inaccurate estimations of carbon stocks and fluxes in aquaculture pond systems.

Organic carbon mineralization refers to the process by which microorganisms transfer electrons from organic substrates to electron acceptors and obtain the energy produced during this process (Stams et al., 2006). In organic-rich aquatic ecosystems such as wetlands, lakes, and reservoirs, oxygen is depleted quickly within a few millimeters of the surface sediment (Brodersen et al., 2019; Kostka et al., 2002; Servais et al., 2019), and carbon mineralization is mediated by anaerobic microbial metabolism, including nitrate reduction, manganese reduction, ferric iron [Fe(III)] reduction, sulfate (SO₄²⁻) reduction, and methanogenesis (Lamers et al., 2012). These microbial metabolic pathways are not exclusive and can coexist in various aquatic sediments (Dombrowski et al., 2018).

Microbial Fe(III) reduction can be comparable and even outcompete other microbial metabolic pathways in the sediments of tidal wetlands (Liu et al., 2019; Luo et al., 2020), lakes (Emmerich et al., 2012), rivers (Yu et al., 2012), and paddy soils (Ding et al., 2015; Khan et al., 2019). Although sulfate reduction and methanogenesis have been widely reported in aquaculture pond systems (Hyun et al., 2013; Nho et al., 2018; Zhou et al., 2022), few studies have focused on Fe(III) reduction and its role in carbon mineralization in aquaculture pond systems. Indeed, aquaculture pond sediments have comparable or higher Fe(III) content than other aquatic sediments (Kim et al., 2020; Lemonnier et al., 2021; Mok et al., 2021). It is therefore reasonable to expect that microbial Fe(III) reduction also plays an essential role in aquaculture pond sediments, although there is currently a lack of field data to support this hypothesis. Iron reduction not only plays a key role in greenhouse gas emissions (Hyun et al., 2009; Neubauer et al., 2005) but also has a significant impact on the energy and nutrient flow and the adsorption and co-precipitation of trace metals (Burton et al., 2008; Johnston et al., 2011). Clarifying microbial Fe(III) reduction and its relationship with sulfate reduction and methanogenesis could contribute to a better understanding of the biogeochemical Fe and C cycling in aquaculture pond sediments.

Farming activities can significantly alter sediment C cycling in aquaculture pond systems (Chanda et al., 2019; Ma et al., 2018; Yang et al., 2018). Little is known about how farming activities affect the rates of microbial Fe(III) reduction in aquaculture systems. Farming activities can modify the availability and lability of organic substrates (Ali et al., 2021; Mulat et al., 2016; Sabu et al., 2022). For instance, in grass carp aquaculture ponds, carp feeding has been found to increase dissolved organic carbon (DOC) concentrations in sediments by 2–5-fold (Chen et al., 2015). Additionally, in a shrimp pond in New Caledonia, the protein content increased from 3.8 to 5.9 mg g⁻¹ from the initial to last stages of shrimp farming, while the lipid content increased from 1.2 to 3.0 mg g⁻¹ (Pusceddu et al., 2011). Furthermore, farming activities can modify the availability of Fe(III). Since oxygen concentrations are sometimes too low to maintain shrimp survival due to intensive aquaculture activities, aerators are widely used in aquaculture ponds during farming (Reis et al., 2021). The application of aerators can significantly elevate oxygen concentrations in aquaculture pond sediments, which can stimulate Fe(II) oxidation and Fe(III) replenishment (Chen, Hall, et al., 2020). Overall, farming activities have the potential to alter the organic substrate and electron acceptors of microbial Fe(III) reduction; and we thus hypothesized that the rates of microbial Fe(III) reduction may also vary across farming stages in aquaculture pond sediments.

Salinity is also an important environmental driver that affects the rates and pathways of carbon mineralization (Luo et al., 2019). Altered salinity could influence carbon mineralization by changing sulfate concentrations, mineral availability, microbial activities, and substrate quantity and quality (Herbert et al., 2015). Previous studies have suggested that increasing salinity could promote sulfate reduction and suppress methanogenesis in aquaculture pond systems (Alongi et al., 1999). This occurs because microbial sulfate reduction is a more energetically favorable process than methanogenesis (Froelich et al., 1979). A relatively unexplored question is how microbial Fe(III) reduction responds to changes in salinity in aquaculture pond systems. A study conducted in tidal wetland

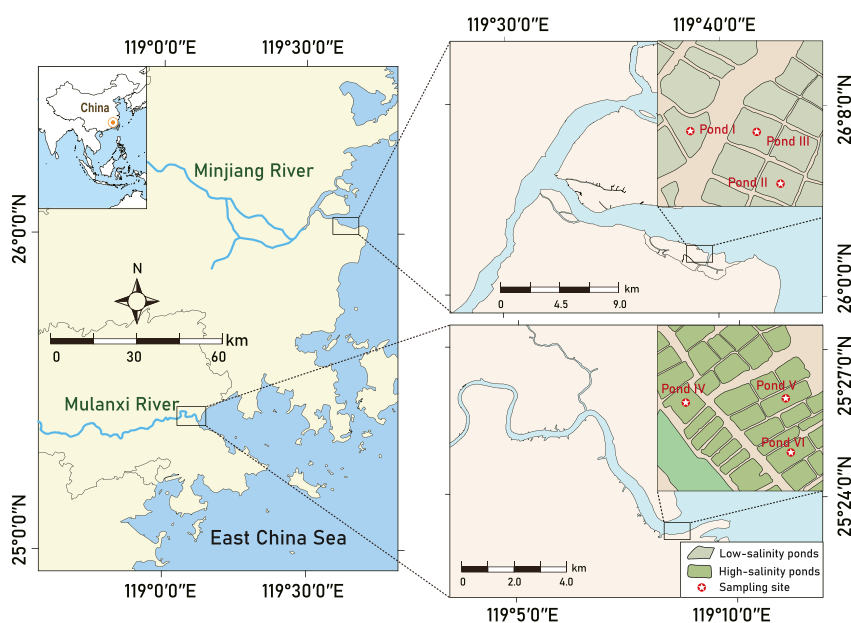


Figure 1. Location of the selected aquaculture ponds in the Minjiang and Mulanxi estuaries near the East China Sea. Three shrimp ponds were selected in the Minjiang Estuary (with a salinity of 2–4 mg g⁻¹; pond I, II, III) and were referred to as “low-salinity” ponds. Three other shrimp ponds were selected in the Mulanxi Estuary (salinity of 14–16 mg g⁻¹; pond IV, V, VI) and were referred to as “high-salinity” ponds.

systems suggested that an increase in salinity of 10 mg g⁻¹ reduced Fe(III) reduction rates by 95% because the activities of iron reducers were suppressed by increasing sulfate reduction (Weston et al., 2006). In contrast, a laboratory study reported that Fe(III) reduction rates increased with increasing porewater Cl⁻ concentrations (0–50 mmol L⁻¹) because increased ionic strength increased the availability of Fe(III) (hydro)oxides (Schoepfer et al., 2014). These inconsistent mechanisms led to an uncertain response of Fe(III) reduction to salinity. Salinity differs highly among coastal aquaculture ponds; thus, identifying the rates of microbial Fe(III) reduction in aquaculture ponds with different salinities may be beneficial for understanding the spatial variation of rates and pathways of carbon mineralization among coastal aquaculture ponds.

To address these gaps, we conducted field investigations in the sediments of aquaculture shrimp (*Litopenaeus vannamei*) ponds in two estuaries with great differences in salinity across pre-farming, farming, and post-farming stages. The major objectives of this study were to explore the effects of aquaculture farming activities and salinity on microbial Fe(III) reduction and its role in carbon mineralization in aquaculture pond systems. We hypothesized that (a) aquaculture farming activities increased the rates of carbon mineralization because of the introduction of aquafeeds; (b) aquaculture farming activities stimulated the contribution of Fe(III) reduction due to a replenishment of Fe(III); (c) high-salinity ponds had higher carbon mineralization rates than low-salinity ponds because more electron acceptors, that is, sulfate, were available; and (d) high-salinity ponds had lower Fe(III) reduction contribution than low-salinity ponds because of intense competition with sulfate reduction.

2. Materials and Methods

2.1. Study Site

The study was conducted in the Minjiang Estuary (26°00'N–26°05'N, 119°30'E–119°41'E) and Mulanxi Estuary (25°23'N–25°25'N, 119°08'E–119°12'E) in Southeast China (Figure 1). The climate in both estuaries comprises subtropical marine monsoons. The average air temperatures of the Minjiang and Mulanxi estuaries are 19.6 and 20.2°C, respectively, and the average precipitation is 1,350 and 1,400 mm, respectively (www.weather.com.cn). Many monoculture aquaculture shrimp (*L. vannamei*) ponds are distributed in the two estuaries, which were all converted from coastal tidal wetlands 7–9 years ago.

Table 1

Location, Stocking Density, Feed Conversion Rate, Yield, Pond Size, Maximum Water Depth, Sediment Texture, and Bulk Density in Aquaculture Ponds in the Minjiang and Mulanxi Estuaries in Southeast China

	Minjiang estuary (low-salinity ponds)			Mulanxi estuary (high-salinity ponds)		
	Pond I	Pond II	Pond III	Pond IV	Pond V	Pond VI
Latitude	26°00'58"N	26°00'56"N	26°01'01"N	25°22'58"N	25°22'58"N	25°22'52"N
Longitude	119°39'25"E	119°39'38"E	119°39'35"E	119°08'26"E	119°08'39"E	119°08'40"E
Stocking density (tails hm ⁻²)	130 × 10 ⁴	130 × 10 ⁴	130 × 10 ⁴	130 × 10 ⁴	130 × 10 ⁴	130 × 10 ⁴
Feed conversion rate	1.48	1.42	1.56	1.49	1.57	1.63
Yield (kg m ⁻³)	12.4	11.8	11.5	12.2	12.7	13.0
Pond size (hm ²)	1.39	1.48	1.33	1.38	1.21	1.26
Maximum water depth (m)	1.75	1.63	1.84	1.62	1.82	1.74
Sand (%)	9.60 ± 0.28	10.64 ± 3.63	7.36 ± 0.77	10.45 ± 2.39	10.26 ± 1.06	9.93 ± 3.06
Slit (%)	76.24 ± 0.72	77.49 ± 2.77	79.03 ± 2.54	77.56 ± 2.53	77.46 ± 1.44	76.46 ± 2.18
Clay (%)	14.16 ± 0.89	11.87 ± 1.35	13.61 ± 2.65	11.99 ± 1.79	12.28 ± 0.54	13.61 ± 0.93
Bulk density (g cm ⁻³)	1.30 ± 0.20	1.29 ± 0.01	1.37 ± 0.02	1.34 ± 0.23	1.32 ± 0.21	1.33 ± 0.16

The salinity of the two estuaries varies greatly. Studies on the ponds from the two estuaries may therefore provide important insights into the ecosystem response of aquaculture ponds to changes in salinity. Moreover, *L. vannamei* is a euryhaline shrimp species that grows well in all ponds. We selected three shrimp ponds in the Minjiang Estuary (with a salinity of 2–4 mg g⁻¹) and referred to them as “low-salinity” ponds. Three other shrimp ponds were selected in the Mulanxi Estuary (salinity of 14–16 mg g⁻¹) and were referred to as “high-salinity” ponds. To isolate the effects of aquaculture farming practices and salinity, the selected ponds were similar in size, maximum water depth, sediment texture, bulk density, and were maintained by consistent aquaculture management practices such as stocking density (Table 1).

Aquaculture farming management was consistent for all the ponds during the experimental period from April to December 2018. On April 2, 2018, water was introduced into the ponds from nearby estuaries, and no additional artificial disturbance occurred during the pre-farming stage (April 3 to May 4, 2018). On May 5, 2018, shrimp larvae were released into the ponds for the farming stage. During the farming stages (May 5–17 November 2018), commercial aquatic feed pellets (including crude protein 31.1%, crude fat 6.8%, moisture 8.7%, ash 5.3%, and fiber 1.1%) were added to the ponds twice a day. Shrimps were harvested from November 12 to 17, 2018. During the post-farming stage (November 18 to December 20, 2018), aquaculture wastewater remained in the ponds, and no additional artificial disturbance occurred.

2.2. Sediment and Porewater Collection

In 2018, sediment sampling was conducted at the pre-farming (April 25th), farming (July 21st), and post-farming (December 11th) stages in all the shrimp ponds. During the sediment sampling, triplicate polyvinyl chloride tubes (length, 15 cm; inner diameter, 10 cm) were randomly inserted into the sediments. The sampling depth was 0–10 cm as this layer is affected the most by aquaculture farming activities (Suárez-Abelenda et al., 2014; Tho et al., 2011). The sediments were bubbled with nitrogen (N₂) and closed with silicone gaskets on both ends before being stored on ice and transferred to the laboratory. The sediment samples were pooled, homogenized, and sieved (2 mm mesh size) in an anaerobic glove bag. The sediment subsamples for incubation and molecular genetics analyses were stored at 4 and –20°C, respectively. Porewater samples were extracted by centrifuging the sediment subsamples at 4,000 × g for 5 min. Porewater samples for NO₃⁻, NH₄⁺, and SO₄²⁻ determination were filtered through a 0.22 μm filter with a cellulose acetate syringe filter, and those for DOC determination were filtered through a 0.45 μm filter with a glass fiber filter. All porewater samples were stored at 4°C before further analysis.

2.3. Sediment Properties Analyses

Sediment total organic carbon (TOC) and total nitrogen (TN) were measured using a CN-elemental analyzer with detection limits of 0.02 mg g⁻¹ (Vario MAX CN, Germany). Prior to assessing the TOC measurements, the sediments were leached with 10% HCl to remove inorganic carbon (Hou et al., 2013). The sediment C:N ratios refers to the TOC versus TN ratio. Salinity was detected using a salinity meter (SALT 6+, Eutech Instruments, Thermo Fisher Scientific, USA), and the unit of salinity was given as mg g⁻¹ (i.e., absolute salinity; Millero, 2010; Millero et al., 2008). Sediment oxidation-reduction potential (ORP) was detected using an ORP meter (FJA-6, Nanjing Chuan-Di Instruments & Equipment Co., Ltd., China; detection limit = 0.1 mV). The ORP of surface sediments was measured when the pond aerators were not operational. The SO₄²⁻ concentrations in the porewater were analyzed using an ICS-2000 Dionex ion chromatograph (Thermo Fisher Scientific) with a detection limit of 2 μmol L⁻¹. The DOC concentrations were analyzed using a TOC analyzer (TOC-VCPH, Shimadzu, Tokyo, Japan) with a detection limit of 2 μmol L⁻¹. The dissolved inorganic carbon (DIC) concentrations were measured using headspace method by collected CO₂ through acidifying porewater to pH = 2.0 with 10% ultrapure HCl (Stainton, 1973). The ammonia (NH₄⁺) and nitrate (NO₃⁻) concentrations in the porewater were determined using a continuous flow analyzer (San++, Skalar Analytical) with detection limits of 2 and 1 μmol L⁻¹, respectively.

Bioavailable Fe(II) and Fe were extracted with 0.5 mol L⁻¹ of HCl and a mixture of 0.5 mol L⁻¹ of HCl and 100 g L⁻¹ of hydroxylamine, respectively (Kostka & Luther III, 1994). The Fe content was determined by the 1,10-phenanthroline method using UV spectrophotometry (UV-2450, Shimadzu, Japan) (APHA, 2005). The Fe(III) content was calculated as the difference between bioavailable Fe and Fe(II) contents. Total reduced sulfur (TRS) was extracted using a 6 mol L⁻¹ HCl solution plus 0.1 mol L⁻¹ of ascorbic acid (Burton et al., 2008). The hydrogen sulfide (ΣH₂S) concentrations were determined by the methylene blue method using UV spectrophotometry (Cline, 1969). The S content in ferrous sulfide (FeS) was estimated based on the difference in the S content between TRS and ΣH₂S (Kostka et al., 2002). The Fe content in FeS was calculated using the stoichiometric relationship between Fe and S in FeS (i.e., Fe:S = 1:1). The non-sulfidic Fe(II) content was calculated based on the difference in the Fe content between Fe(II) and FeS (Luo et al., 2014). The Fe(II), Fe(III), and TRS recovery rates were assessed in triplicate using FeCO₃, ferric oxide-hydroxide, and Na₂S and were found to be 95%–104%, 97%–103%, and 89%–108%, respectively.

2.4. Fluorescence Measurements

Three-dimensional emission matrix (3D-EEM) fluorescence measurements were assessed using a fluorescence spectrophotometer (Hitachi F-7100, Tokyo, Japan). The scanning ranges of the excitation (Ex) and emission wavelengths (Em) were 200–450 nm (interval: 5 nm) and 210–550 nm (interval: 1 nm), respectively. The fluorescence spectra samples were corrected by subtracting the Milli-Q water blank signals and normalized by the Raman peak at 350 nm of Milli-Q water (Lawaetz & Stedmon, 2009). The negative fluorescence intensity values were set to 0, and the Rayleigh scattering peaks were trimmed. A total of 54 3D-EEM datasets were then modeled with a parallel factor analysis (PARAFAC) in MATLAB 2019 with the DOMFluor toolbox version 1.7 (Stedmon & Bro, 2008). Three fluorescent components were identified by split-half validation and visual inspection (Stedmon et al., 2003). The normalized maximum fluorescence intensity (F_{\max}) of each component was used to estimate quantitative and qualitative variations (Stedmon & Markager, 2005).

2.5. Molecular Genetic Analyses

Soil DNA was extracted from 0.25 g of fresh soil using PowerSoil DNA Extraction Kits (MoBio Laboratory, CA, USA), according to the manufacturer's instructions. The abundance of the *mcrA* gene (methanogen) was determined using the primers *mcrA*-F and *mcrA*-R (Steinberg & Regan, 2009). The *dsrA* gene (sulfate reducer) was targeted using the primers *dsrA* 290F and *dsrA* 660R (Pereyra et al., 2010). Iron reducers have no functional genes (Li et al., 2011); however, based on investigations of 16S rRNA gene sequences, *Geobacter* accounted for 84.5% of the total identified iron reducers in the aquaculture shrimp pond sediments. Thus, we selected *Geobacter* as a proxy for iron reducers in this study. The abundance of *Geobacter* was targeted using the primers 494F and 825R (Holmes et al., 2002). qPCR assays were performed using a real-time PCR system (Applied Biosystems 7500, Thermo Fisher Scientific Inc., USA). Further details on the molecular genetics analyses can be found in the study by Liu et al. (2019).

Table 2

Sediment and Porewater Properties (Mean ± Standard Deviation; n = 9) in the Low-Salinity and High-Salinity Ponds Across the Three Aquaculture Farming Stages

Properties	Ponds	Stages			Factor	Two-way ANOVA		
		Pre-farming	Farming	Post-farming		Stage	Pond	Interaction
Salinity (mg g ⁻¹)	Low-salinity	3.24 ± 1.06Ab	2.50 ± 1.50Ab	2.70 ± 1.08Ab	<i>F</i>	0.999	439.799	0.451
	High-salinity	15.57 ± 2.19Aa	14.48 ± 3.32Aa	16.03 ± 2.93Aa	<i>P</i>	0.376	<0.001	0.639
Sulfate (mmol L ⁻¹)	Low-salinity	2.84 ± 1.52Ab	3.12 ± 1.20Ab	2.49 ± 1.37Ab	<i>F</i>	1.830	464.871	1.532
	High-salinity	16.03 ± 2.31Aa	14.12 ± 1.72Aa	13.84 ± 3.24Aa	<i>P</i>	0.171	<0.001	0.226
ORP ^a (mV)	Low-salinity	-150.5 ± 48.6Aa	-142.2 ± 63.5Aa	-169.1 ± 33.5Aa	<i>F</i>	0.136	19.037	0.944
	High-salinity	-207.9 ± 39.6Ab	-210.6 ± 36.1Ab	-198.7 ± 32.2Ab	<i>P</i>	0.873	<0.001	0.396
TOC (mg g ⁻¹)	Low-salinity	20.12 ± 1.48Ab	21.23 ± 1.18Ab	20.42 ± 1.74Ab	<i>F</i>	2.986	6.040	0.031
	High-salinity	21.15 ± 1.38Aa	22.34 ± 1.25Aa	21.28 ± 1.83Aa	<i>P</i>	0.60	0.018	0.971
C:N ratios	Low-salinity	10.89 ± 1.17Ab	10.13 ± 1.20Ab	10.28 ± 0.70Ab	<i>F</i>	2.996	17.347	0.031
	High-salinity	11.96 ± 0.80Aa	11.21 ± 0.93Aa	11.41 ± 0.91Aa	<i>P</i>	0.059	<0.001	0.970
DOC (mmol L ⁻¹)	Low-salinity	11.46 ± 2.65Ba	15.34 ± 2.19Aa	11.89 ± 0.71Ba	<i>F</i>	17.685	9.865	0.419
	High-salinity	9.97 ± 2.17Bb	13.10 ± 1.66Ab	10.79 ± 1.21Bb	<i>P</i>	<0.001	0.003	0.660
DIC (mmol L ⁻¹)	Low-salinity	1.48 ± 0.23Ba	2.42 ± 0.28Aa	1.64 ± 0.35Ba	<i>F</i>	64.159	8.749	0.318
	High-salinity	1.35 ± 0.26Bb	2.19 ± 0.16Ab	1.38 ± 0.23Bb	<i>P</i>	<0.001	0.005	0.729
NO ₃ ⁻ (μmol L ⁻¹)	Low-salinity	0.81 ± 0.26Ba	1.73 ± 0.45Aa	2.33 ± 0.52Aa	<i>F</i>	52.004	11.825	0.242
	High-salinity	0.51 ± 0.27Bb	1.34 ± 0.38Ab	1.84 ± 0.55Ab	<i>P</i>	<0.001	0.001	0.786
NH ₄ ⁺ (μmol L ⁻¹)	Low-salinity	55.78 ± 10.09Bb	165.25 ± 24.68Ab	178.00 ± 32.32Ab	<i>F</i>	155.402	12.412	0.720
	High-salinity	69.44 ± 9.79Ba	188.57 ± 32.36Aa	211.16 ± 25.85Aa	<i>P</i>	0.001	0.001	0.492
Fe(III) (μmol g ⁻¹)	Low-salinity	29.98 ± 7.26Ba	74.19 ± 14.78Aa	29.55 ± 7.74Ba	<i>F</i>	93.768	44.772	7.926
	High-salinity	19.27 ± 4.13Bb	45.04 ± 8.91Ab	21.75 ± 5.40Bb	<i>P</i>	<0.001	<0.001	0.001
Non-sulfidic Fe(II) (μmol g ⁻¹)	Low-salinity	41.06 ± 6.83Aa	13.29 ± 4.91Ba	38.54 ± 12.61Aa	<i>F</i>	46.121	26.408	2.322
	High-salinity	29.88 ± 12.07Ab	7.56 ± 4.99Bb	21.03 ± 1.82Ab	<i>P</i>	<0.001	<0.001	0.109
FeS (μmol g ⁻¹)	Low-salinity	20.96 ± 3.89Ab	11.86 ± 2.54Bb	27.36 ± 2.82Ab	<i>F</i>	20.739	24.622	1.652
	High-salinity	38.31 ± 13.41Aa	18.64 ± 5.71Ba	41.98 ± 14.15Aa	<i>P</i>	<0.001	<0.001	0.202
Fe(III):Fe(II) ratios ^b	Low-salinity	0.49 ± 0.14Ba	3.07 ± 0.86Aa	0.47 ± 0.18Ba	<i>F</i>	123.538	16.579	8.214
	High-salinity	0.31 ± 0.12Bb	1.86 ± 0.65Ab	0.36 ± 0.10Ba	<i>P</i>	<0.001	<0.001	0.001

Note. Different uppercase letters indicate significant differences across the three aquaculture farming stages. Different lowercase letters indicate significant differences between the low- and high-salinity ponds within a single stage.

^aOxidation-reduction potential. ^bFe(II) contains Fe sulfides and non-sulfidic Fe(II).

2.6. Sediment Incubation

We applied anaerobic incubation to determine the rates of microbial Fe(III) and sulfate reduction, methanogenesis, and carbon mineralization because our ORP data showed that the aquaculture pond sediments were anaerobic (Table 2). The rates of microbial Fe(III) and sulfate reduction, methanogenesis, and carbon mineralization have previously been quantified by sediment incubation (Luo et al., 2020; Neubauer et al., 2005).

For the rates of microbial Fe(III) and sulfate reduction, ~5 g soil subsamples were slurried with deoxygenated in situ surface water (2:1, w:w) in vials under a nitrogen atmosphere, purged with nitrogen gas for 5 min, crimp-sealed, and incubated in the dark at room temperature (25°C) for 4 days. To determine the reduction rates of Fe(III), sodium molybdate solution was added to the soils to inhibit microbial sulfate reduction at a final concentration of 20 mmol L⁻¹ (Luo et al., 2020). During incubation, subsamples were sacrificed to determine the accumulation of Fe(II) and TRS. The Fe(III) reduction rates were determined by the linear regression of Fe(II) concentration with time (Chen & Jiang, 2016; Hyun et al., 2009; Kostka et al., 2002; Vermeire et al., 2019). The rates of microbial sulfate reduction were determined by the production of TRS (Kristensen et al., 2000;

Lukawska-Matuszewska et al., 2019; Luo et al., 2016). We cannot rule out the possibility that rapid reoxidation of TRS to SO_4^{2-} was taking place in our slurries, leading to an underestimate of the role of sulfate reduction. However, given the anaerobic nature of the slurries, we assume that the reoxidation of TRS to SO_4^{2-} was likely minimal in this experiment (Kristensen et al., 2011). The rates of Fe(III) and sulfate reduction were determined by regressing Fe(II) ($r^2 > 0.84$) and TRS ($r^2 > 0.81$) production against incubation time.

To measure the rates of methanogenesis and carbon mineralization, triplicated sediment samples of approximately 20 g were slurried with deoxygenated in situ surface water (2:1, w:w) in an N_2 atmosphere, purged with N_2 gas for 5 min, crimp-sealed, and incubated in 100 mL glass incubation bottles with a precise volume measurement in the dark at ambient temperature. Gas samples were collected from the headspace on days 0, 1, 2, and 3 of incubation and analyzed for CO_2 and CH_4 concentrations. Before sampling, each bottle was shaken on a rotary shaker at 240 rpm for 1 hr to drive the escaped CO_2 and CH_4 into the headspaces. After each gas sample was collected, the incubation bottles were backfilled with N_2 (equal to the sampling amount) to re-establish normal atmospheric pressure. The CO_2 and CH_4 concentrations were measured using a gas chromatograph fitted with a flame-ionization detector and a CO_2 reforming furnace (GC2010, Shimadzu, Japan). The measured CO_2 and CH_4 concentrations were corrected for pH, headspace pressure, and temperature (Ye et al., 2012). The rates of methanogenesis and carbon mineralization were estimated from the cumulative production of CH_4 ($r^2 > 0.90$) and CO_2 plus CH_4 over time ($r^2 > 0.90$), respectively.

To partition the carbon mineralization, the rates of Fe(III) and sulfate reduction and methanogenesis were normalized with the carbon unit ($\mu\text{mol C g}^{-1} \text{d}^{-1}$) using the theoretical stoichiometry of Fe:C = 4:1, S:C = 1:2, and C- CH_4 :C = 1:2 (Kostka et al., 2002; Neubauer et al., 2005).

2.7. Data Analysis

All analyses were conducted using the software R (version 4.0.3; R Core Team, 2013). A two-way analysis of variance (ANOVA) was used to test the effects of aquaculture farming activities and salinity on the rates of carbon mineralization and microbial metabolic pathways, sediment and porewater properties, PARAFAC components, and microbial abundance at a significance level of $p < 0.05$. Prior to performing the ANOVA, all the datasets were analyzed to identify whether they met the assumptions of normality (Shapiro-Wilk test). The data were \log_{10} transformed if the transformation substantially improved their distribution. The ANOVA was performed using the *aov* function. Multiple comparisons across the three aquaculture farming stages were performed using one-way ANOVAs followed by Tukey's HSD *post-hoc* test. Pairwise comparisons between the low- and high-salinity ponds were performed using paired-sample *t*-tests.

Linear regression models were used to examine the relationships between the carbon mineralization rates and DOC concentrations, C3:(C1+C2+C3) ratios, and C:N ratios, with significance set at $p < 0.05$. A redundancy analysis was performed using the packages *vegan* and *rdacca.hp* to determine the main factors that affected the changes in the microbial metabolic pathway (Lai et al., 2022; Oksanen et al., 2007).

A hypothesized structural equation model was built to assess the impact of salinity on the rates and pathways of carbon mineralization using the *lavaan* package (Rosseel, 2012). The hypothesized structural equation model was based on the proposition that salinity could drive carbon mineralization by influencing environmental factors (Figure S1 in Supporting Information S1). Our hypotheses were that (a) salinity affected sulfate concentrations, Fe(III) content, and organic substrate characteristics; (b) sulfate concentrations and Fe(III) content further affected microbial metabolic pathways; and (c) Fe(III) content, sulfate concentrations, organic substrate characteristics, and microbial metabolic pathways affected carbon mineralization rates. After the initial model had been established, we went through the processes of adding and removing pathways and variables to achieve the final model. Goodness of fit was assessed based on a chi-square test, comparative fit index, and Akaike information criterion values.

3. Results

3.1. Sediment and Porewater Properties

The salinity in the ponds of the Minjiang Estuary ranged from 2.50 to 3.24 mg g^{-1} , while the salinity in the ponds of the Mulanxi Estuary ranged from 14.48 to 16.03 mg g^{-1} (Table 2). The sulfate concentrations in

the porewater were lower in the low-salinity ponds of 2.50–3.24 mmol L⁻¹, than the high-salinity ponds, of 14.48–16.03 mmol L⁻¹ (Table 2). Both salinity and the porewater sulfate concentrations were comparable across three aquaculture farming stages. The sediment ORP ranged from -210.6 to -142.2 mV (Table 2). High-salinity ponds had lower ORP than low-salinity ponds (Table 2). The TOC content ranged from 20.12 to 22.34 mg g⁻¹ (Table 2). The TOC content was comparable across the three aquaculture farming stages. High-salinity ponds had higher TOC content than low-salinity ponds (Table 2). Sediment C:N ratios ranged from 10.13 to 11.96 (Table 2). Lower sediment C:N ratios were observed in the low-salinity ponds than in the high-salinity ponds, while sediment C:N ratios did not significantly change across the three aquaculture farming stages. The DOC concentrations ranged from 9.97 to 15.34 mmol L⁻¹, while the DIC concentrations ranged from 1.35 to 2.42 mmol L⁻¹ (Table 2). Higher DOC and DIC concentrations occurred in the farming stages than in the pre-farming and post-farming stages, whereas higher DOC and DIC concentrations were observed in the low-salinity ponds than in the high-salinity ponds (Table 2). The NO₃⁻ concentrations in the porewater ranged from 0.51 to 2.33 μmol L⁻¹, while the NH₄⁺ concentrations in the porewater ranged from 55.78 to 211.16 μmol L⁻¹ (Table 2). Higher NH₄⁺ concentrations were observed in the high-salinity ponds than in the low-salinity ponds, whereas higher NO₃⁻ concentrations were observed in the low-salinity ponds than in the high-salinity ponds. Fe(III) content ranged from 19.27 to 74.19 μmol g⁻¹, while non-sulfidic Fe(II) and FeS contents ranged from 7.56 to 41.06 μmol g⁻¹ and 11.86–41.98 μmol g⁻¹, respectively (Table 2). Higher Fe(III) content was observed during farming than before and after farming, with Fe(III):Fe(II) ratios being greater than 1 during farming. In contrast, higher non-sulfidic Fe(II) and FeS contents were observed before and after farming than during farming, with Fe(III):Fe(II) ratios being smaller than 1 before and after farming. The non-sulfidic Fe(II) content was higher in the low-salinity ponds than in the high-salinity ponds, whereas the FeS content was lower in the low-salinity ponds than in the high-salinity ponds.

3.2. Rates and Pathways of Carbon Mineralization

Microbial Fe(III) reduction rates ranged from 0.24 to 1.52 μmol g⁻¹ d⁻¹ (Figure 2a). Across three aquaculture farming stages, microbial Fe(III) reduction rates were higher in the farming stages than in the pre- and post-farming stages. The low-salinity ponds had relatively higher microbial Fe(III) reduction rates than the high-salinity ponds. Sulfate reduction rates ranged from 0.38 to 0.80 μmol g⁻¹ d⁻¹, while methanogenesis rates ranged from 0.00 to 0.05 μmol g⁻¹ d⁻¹ (Figures 2b and 2c). The sulfate reduction and methanogenesis rates were also higher in the farming stages than in the pre- and post-farming stages. Moreover, the sulfate reduction rates were higher in the high-salinity ponds than in the low-salinity ponds, whereas the methanogenesis rates were higher in the low-salinity ponds than in the high-salinity ponds. The carbon mineralization rates ranged from 1.02 to 2.17 μmol g⁻¹ d⁻¹ (Figure 2d). Similar to the microbial metabolic pathways, the carbon mineralization rates were also higher in the farming stages than in the pre- and post-farming stages. The high-salinity ponds had relatively lower carbon mineralization rates than the low-salinity ponds.

On average, Fe(III) reduction (mean: 46.1%) dominated carbon mineralization, followed by sulfate reduction (mean: 39.6%) and methanogenesis (mean: 1.5%; Figure 3). Higher Fe(III) reduction contribution was observed in the farming stages (mean: 56.9%) than in the pre-farming (mean: 40.5%) and post-farming stages (mean: 40.8%; Figure 3). Sulfate reduction contribution was lower during farming (mean: 33.1%) than before (mean: 45.9%) and after farming (mean: 39.7%; Figure 3). Methanogenesis contribution (<3%) was comparable across the aquaculture farming stages in both pond types (Figure 3). The high-salinity ponds (mean: 31.1%) had a relatively lower Fe(III) reduction contribution to carbon mineralization than the low-salinity ponds (mean: 61.1%; Figure 3).

3.3. Microbial Abundance

The abundance of *Geobacter* ranged from 2.13 × 10⁷ to 9.78 × 10⁷ copies g⁻¹ (Figure 4a), while the abundance of *dsrA* ranged from 0.61 × 10⁸ to 5.82 × 10⁸ copies g⁻¹ (Figure 4b). The abundance of *mcrA* ranged from 0.46 × 10⁶ to 1.62 × 10⁶ copies g⁻¹ (Figure 4c). The abundances of *Geobacter* and *dsrA* were higher during farming than before and after farming. The high-salinity ponds had relatively lower *Geobacter* and *mcrA* abundance but higher *dsrA* abundance than the low-salinity ponds.

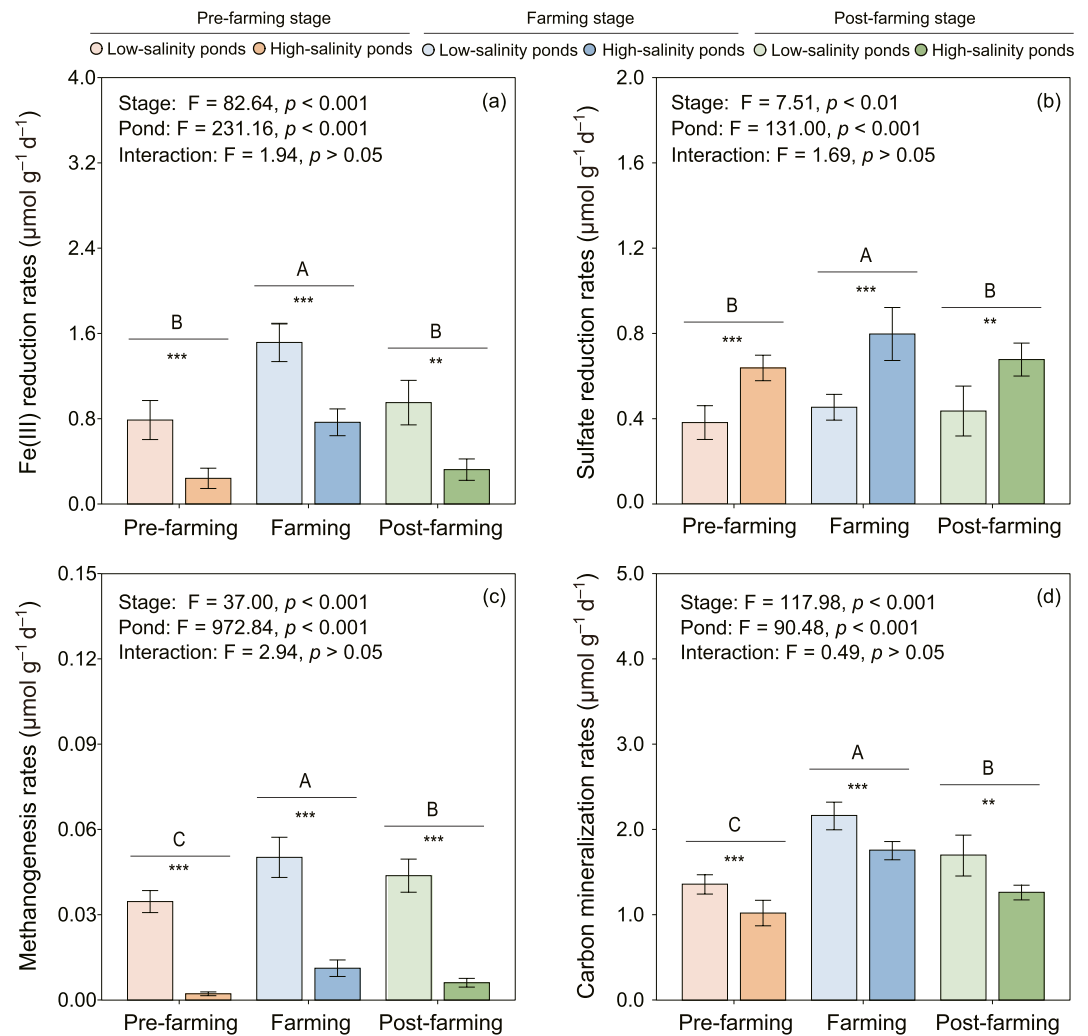


Figure 2. Microbial Fe(III) and sulfate reduction rates (a and b), methanogenesis rates (c), and carbon mineralization rates (d) in the aquaculture shrimp ponds of the Minjiang and Mulanxi estuaries across the three aquaculture farming stages. All data are the mean \pm standard deviation ($n = 9$). Different uppercase letters indicate significant differences across the three aquaculture farming stages. Asterisks denote significant differences between the ponds within one stage ($*p < 0.05$; $**p < 0.01$; $***p < 0.001$).

3.4. PARAFAC Components

Three common fluorescent components (C1–C3) were extracted using 3D-EEM PARAFAC (Figure 5). The positions of the Ex/Em maxima for the three components were 295/430 nm (C1), 230/410 nm (C2), and 285/340 nm (C3).

The F_{max} of C1, C2, and C3 ranged from 0.06 to 0.10, 0.00 to 0.13, and 0.08 to 0.19 Raman Units, respectively (Table 3). The F_{max} of C1 did not change across the farming stages. The F_{max} of C2 decreased from pre- and post-farming to the farming stage, whereas the F_{max} of C3 was higher during farming than before and after farming. The F_{max} of C1, C2, and C3 did not change between the low- and high-salinity ponds.

3.5. Relationships Between the Rates and Pathways of Carbon Mineralization and Environmental Factors

The carbon mineralization rates increased with the DOC concentrations (Figure 6a), increased with the C3:(C1+C2+C3) ratios (Figure 6b), and decreased with the C:N ratios (Figure 6c).

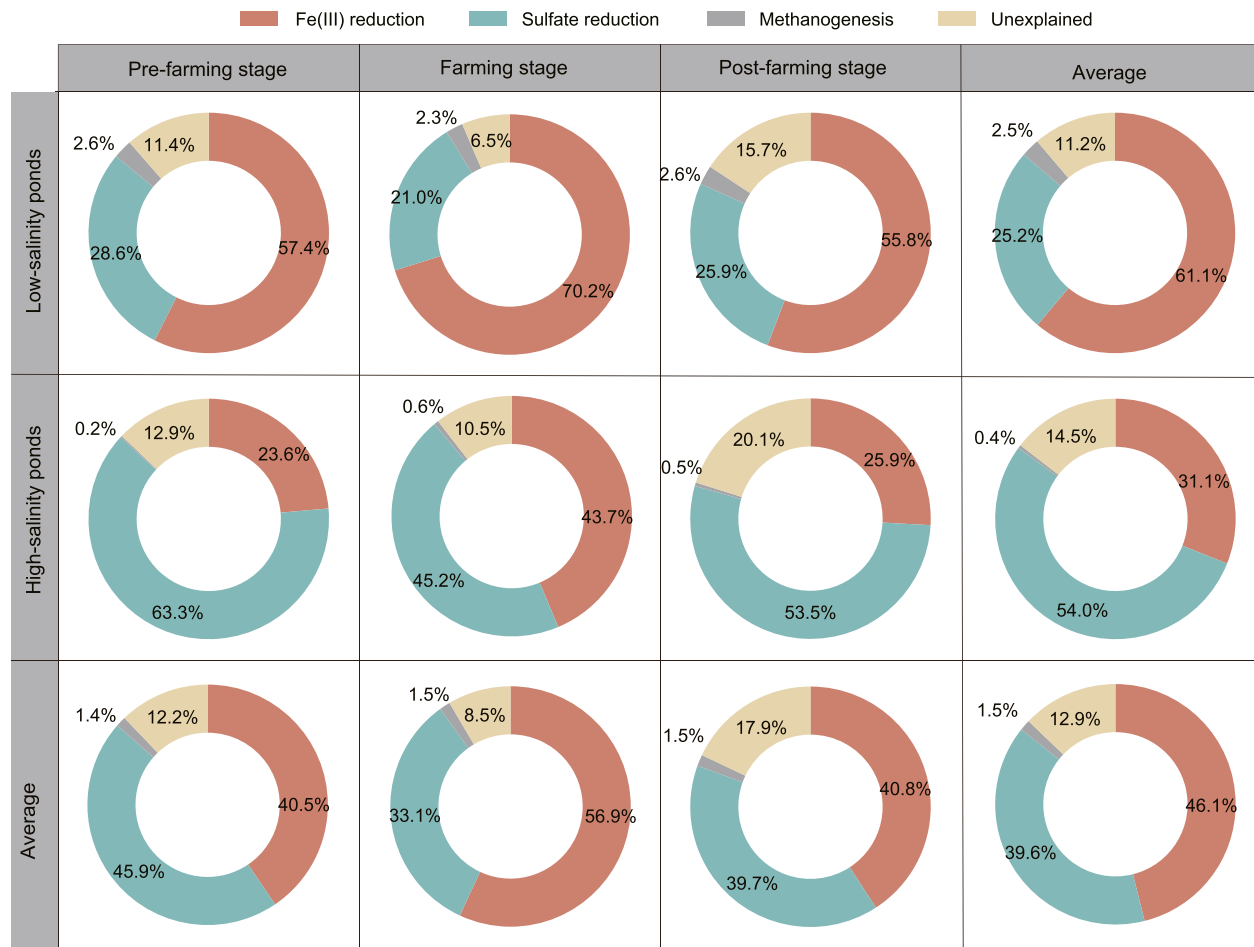


Figure 3. Contributions (%) of Fe(III) and sulfate reduction, methanogenesis, and unexplained pathway to carbon mineralization in the aquaculture shrimp ponds of the Minjiang and Mulanxi estuaries across the three aquaculture farming stages.

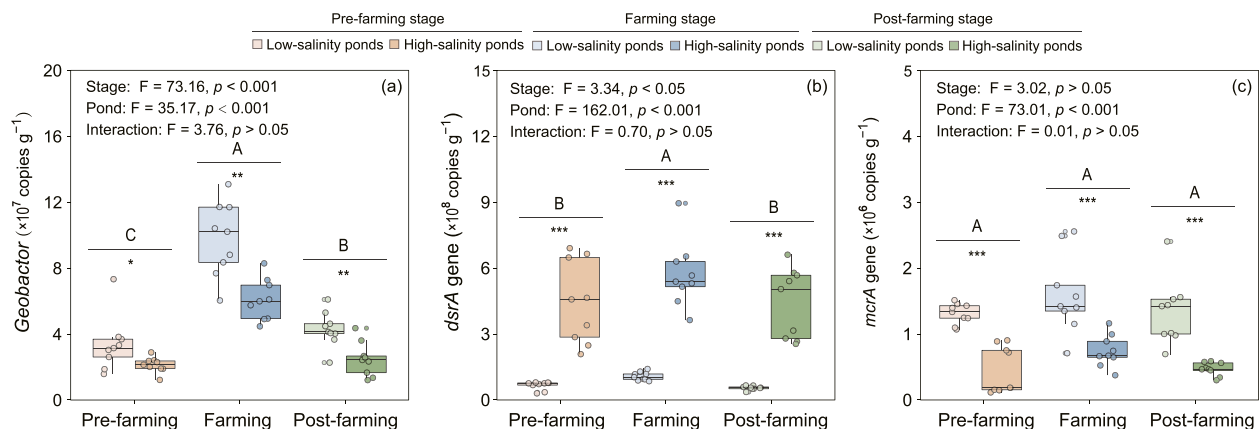


Figure 4. The abundance of *Geobacter* (a), *dsrA* (b), and *mcrA* (c) in the aquaculture shrimp ponds of the Minjiang and Mulanxi estuaries across three aquaculture farming stages. All data are the mean \pm standard deviation ($n = 9$). Different uppercase letters indicate significant differences across the three aquaculture farming stages. Asterisks denote significant differences between the ponds within one stage (* $p < 0.05$; ** $p < 0.01$; *** $p < 0.001$).

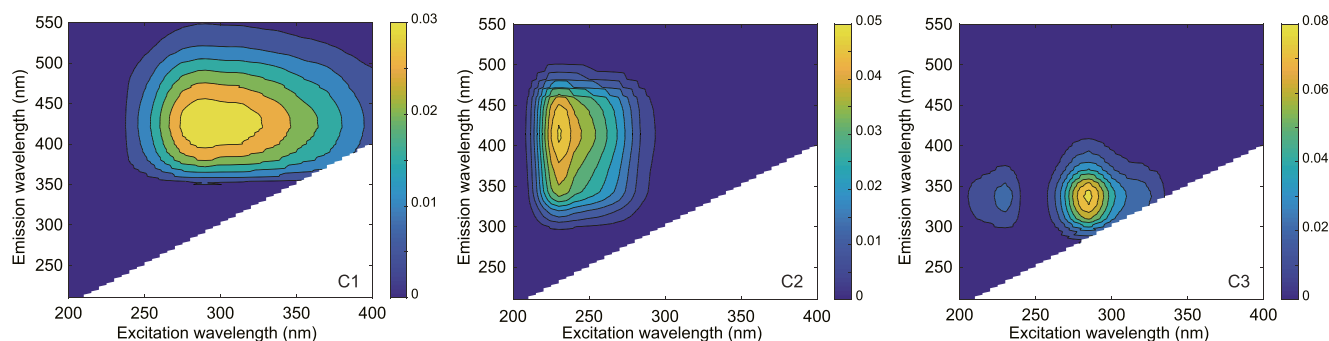


Figure 5. Three-dimensional emission matrix (3D-EEM) contours of the fluorescent components C1–C3 identified using PARAFAC in the aquaculture ponds of the Minjiang and Mulanxi estuaries.

The redundancy analysis suggested that the variations in the microbial metabolic pathways were affected by the concentrations of sulfate, contents of Fe(III) and FeS, and salinity (Figure 7).

The structural equation modeling analysis suggested that salinity indirectly influenced carbon mineralization rates by driving environmental factors (Figure 8). Salinity affected the sulfate concentrations and Fe(III) content, which further affected the partitioning of the microbial metabolic pathways. Salinity further impacted the properties of the organic substrates. Finally, sulfate concentrations, Fe(III) content, the partitioning of the microbial metabolic pathways, and properties of the organic substrates determined the carbon mineralization rates.

4. Discussion

4.1. Carbon Mineralization Across the Aquaculture Farming Stages

In line with Hypothesis I, the aquaculture farming activities induced a sharp stimulation in carbon mineralization in the aquaculture pond sediments at the farming stages compared to the pre- and post-farming stages (Figure 2d). The enhanced carbon mineralization rates may be due to an increase in the quantity and lability of the organic substrates during farming.

The hypothesis that carbon mineralization rates are affected by organic substrate quantity was validated by our results, which showed that DOC concentrations increased by an average of 29% during farming (Table 2) and were correlated with the carbon mineralization rates (Figures 6a and 8). During farming, high aquafeed loads are

Table 3
PARAFAC Component Description and Normalized Maximum Fluorescence Intensity (F_{max}) (Mean \pm Standard Deviation; $n = 9$) in the Low- and High-Salinity Ponds Across the Three Aquaculture Farming Stages

Components and description*	Ponds	Stages			Factor	Two-way ANOVA		
		Pre-farming	Farming	Post-farming		Stage	Pond	Interaction
Humic-like, C1 (Raman Unit)	Low-salinity	0.08 \pm 0.04Aa	0.10 \pm 0.06Aa	0.09 \pm 0.06Aa	<i>F</i>	2.491	1.863	0.181
	High-salinity	0.06 \pm 0.01Aa	0.10 \pm 0.04Aa	0.07 \pm 0.01Aa	<i>P</i>	0.094	0.179	0.835
Fulvic-like, C2 (Raman Unit)	Low-salinity	0.12 \pm 0.05Aa	0.00 \pm 0.01Ba	0.13 \pm 0.07Aa	<i>F</i>	33.764	2.536	1.254
	High-salinity	0.11 \pm 0.01Aa	0.01 \pm 0.01Ba	0.09 \pm 0.06Aa	<i>P</i>	<0.001	0.118	0.297
Tryptophan-like, C3 (Raman Unit)	Low-salinity	0.08 \pm 0.02Ba	0.15 \pm 0.07Aa	0.09 \pm 0.02Ba	<i>F</i>	20.958	13.512	0.158
	High-salinity	0.11 \pm 0.01Ba	0.19 \pm 0.04Aa	0.13 \pm 0.03Ba	<i>P</i>	<0.001	0.071	0.855

Note. *The identities of the components were inferred using the OpenFluor database (<https://openfluor.labcicate.com>). C1 (295/430 nm) can be characterized as a terrigenous humic-like component and is commonly found in marine environments, wastewater, wetlands, and agricultural environments (Graeber et al., 2012; Yan et al., 2020). C2 (230/410 nm) is a fulvic-like component derived from plant material (Coble et al., 1998; Yan et al., 2020). C3 (285/340 nm) is a tryptophan-like component (Murphy et al., 2011). Different uppercase letters indicate significant differences across the three farming stages. Different lowercase letters indicate significant differences between the low- and high-salinity ponds within a single stage.

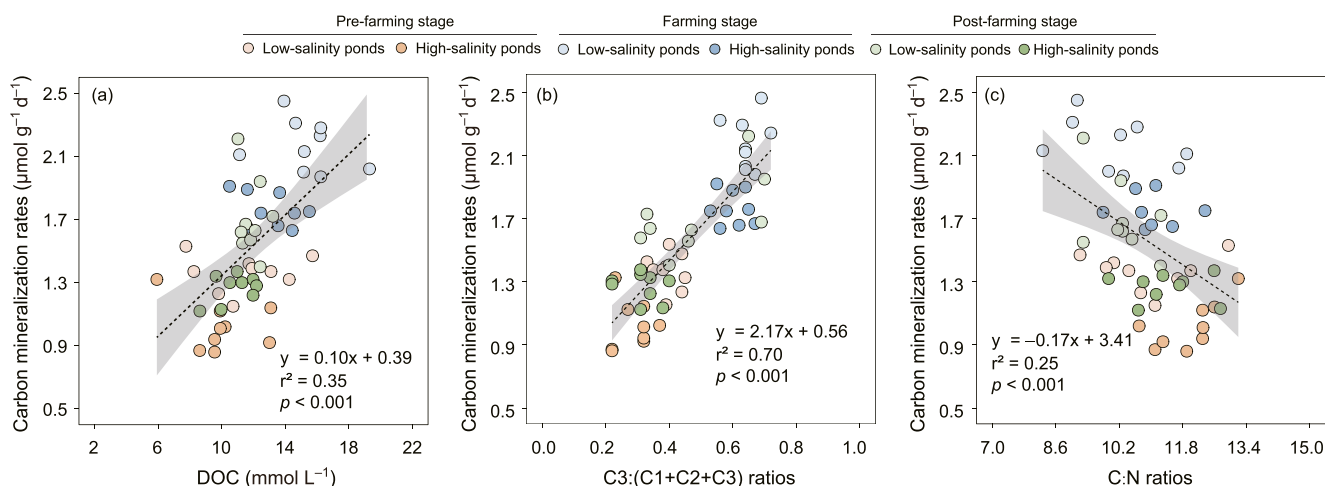


Figure 6. Relationships between the carbon mineralization rates and dissolved organic carbon (DOC) concentrations, C3:(C1+C2+C3) ratios, and C:N ratios. C1, C2, and C3 are fluorescent components derived from the 3D-EEM of PARAFAC.

typically hydrolyzed to DOC, and shrimp excreta is also likely to enrich DOC in low molecular weight, easily assimilable organic compounds (Beardsley et al., 2011). Previous research has also reported similar correlations between carbon mineralization rates and DOC concentrations in pristine ponds and peatlands (Bertora et al., 2018; Holgerson, 2015), suggesting that DOC is bioavailable for most heterotrophic microorganisms. Therefore, an increase in DOC concentrations could explain the elevated carbon mineralization rates in the aquaculture pond sediments during farming.

The effects of the lability of the organic substrates on the carbon mineralization rates were demonstrated by a positive relationship between the carbon mineralization rates and C3:(C1+C2+C3) ratios (Figures 6b and 8). To obtain high-quality aquatic proteins, aquafeed usually contains high protein components, such as peanut and bean dregs (Dawood et al., 2018). These protein-rich aquafeeds were further hydrolyzed into tryptophan, resulting in a significant increase in C3 (Table 3). Heterotrophic microorganisms prefer labile substrates such as tryptophan to recalcitrant substrates (de Melo et al., 2020). Consequently, the introduction of labile organic substrates also contributed to an increase in the carbon mineralization rates during farming.

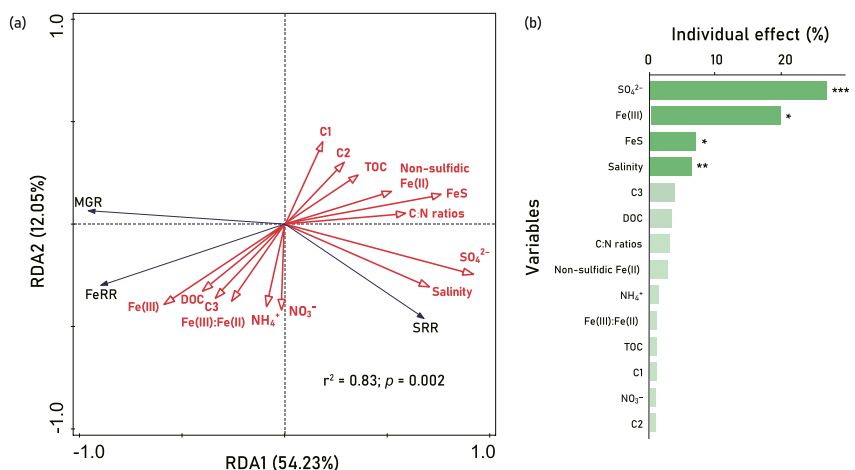


Figure 7. The redundancy analysis (a) showed variations in the rates of the microbial metabolic pathways relative to environmental factors. Panel (b) shows the proportion of each explanatory variable compared to the variations in the rates of the microbial metabolic pathways. The asterisks in panel (b) indicate the significance of each explanatory variable (* $p < 0.05$; ** $p < 0.01$; *** $p < 0.001$). FeRR: Fe(III) reduction rates; SRR: sulfate reduction rates; MGR: methanogenesis rates; C1, C2, and C3 are fluorescence components derived from the 3D-EEM of PARAFAC.

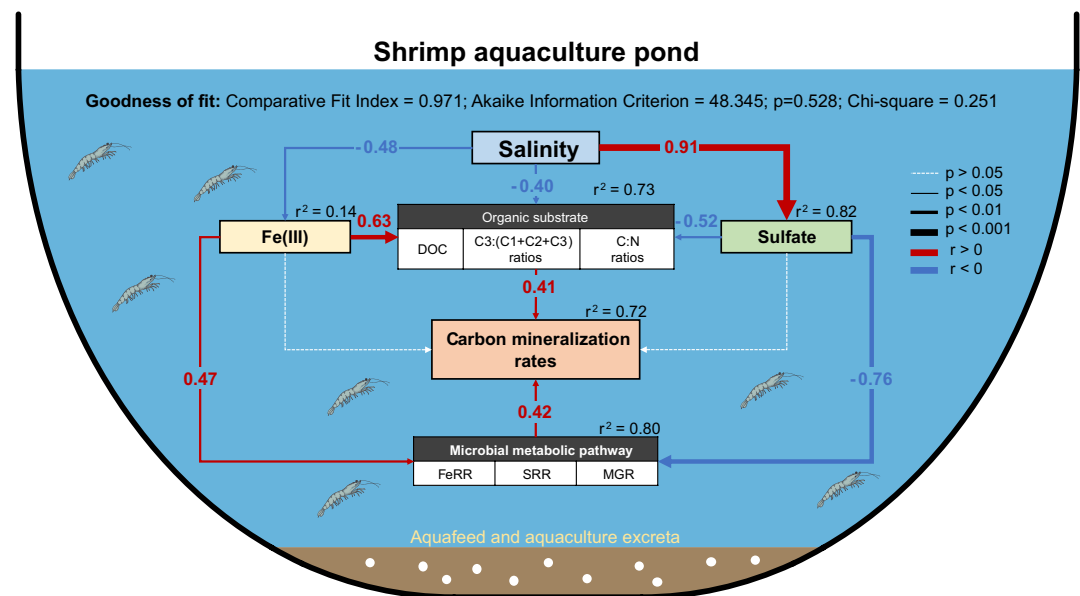


Figure 8. A structural equation model assessing the impact of salinity on the rates and pathways of carbon mineralization. The numbers on the arrows indicate the coefficients, and the arrow widths indicate their significance. The figures next to the variables indicate their explained variance (r^2). FeRR: Fe(III) reduction rates; SRR: sulfate reduction rates; MGR: methanogenesis rates; C1, C2, and C3: a fluorescence component derived from the 3D-EEM of PARAFAC.

4.2. Microbial Fe(III) Reduction Across the Aquaculture Farming Stages

Similar to the carbon mineralization rates (Figure 2d), the rates of microbial Fe(III) increased from before and after farming to during farming (Figures 2a–2c). We further found that the contribution of Fe(III) reduction during farming (56.9%) was higher than those before and after farming (40.5%–40.8%) (Figure 3). In accordance with the contribution of microbial Fe(III) reduction, *Geobacter* abundance showed a greater increase (159%) during farming than before and after farming (Figures 4a–4c). All these results suggested that aquaculture farming activities enhanced microbial Fe(III) reduction.

Consistent with Hypothesis II, the redundancy analysis and structural equation modeling indicated that the promotion for microbial Fe(III) reduction during farming relied on significant changes in Fe(III) content (Figures 7 and 8), which increased by 137% during farming compared to before and after farming (Table 2). The higher content of Fe(III) during farming could be accounted for by the application of aerators, which could bring fresh air oxygen to the surface layer of pond sediments and immediately oxidize Fe(II) to Fe(III) (Chen, Miao, et al., 2020). In line with this, higher Fe(III):Fe(II) ratios (1.86–3.07) were observed during farming compared with before and after farming (0.31–0.49) (Table 2). The newly yielded Fe(III) is mostly amorphous and highly bioavailable, which can supply electron acceptors to iron reducers (Wang et al., 2020). Once Fe(III) is reduced to Fe(II), Fe(II) is immediately re-oxidized to Fe(III) instead of being adsorbed on the surface of Fe(III) (Tong, Wang, et al., 2021; Wang et al., 2021). This was crucial for maintaining high rates of Fe(III) reduction, as the accumulation of Fe(II) may gradually reduce the accessibility of Fe(III) to iron reducers (Weston et al., 2006). Accordingly, our results suggest that rapid Fe(III) replenishment facilitates microbial Fe(III) reduction during farming.

4.3. Carbon Mineralization Rates in Ponds With Different Salinities

In contrast to Hypothesis III, the high-salinity ponds had lower carbon mineralization rates than the low-salinity ponds (Figure 2d). The increases in the sediment C:N ratios as salinity increased may account for the reduction in carbon mineralization rates in the high-salinity ponds (Figures 6c and 8). The increased sediment C:N ratios (i.e., a decrease in N availability) as salinity increased may have been due to increased NH_4^+ release with increasing salinity (Table 2). This is because cations in saltwater (e.g., Na^+ , Ca^{2+} , and K^+) may quickly replace NH_4^+ adsorbed in sediments and then release them into the overlying water (Tully et al., 2019). Heterotrophic microorganisms

prefer organic substrates with a lower C:N ratios because high nitrogen substrates can support rapid microbial metabolism (Redmile-Gordon et al., 2015; Zhang et al., 2020). In contrast, high sediment C:N ratios indicate that the substrate for microbial metabolism may be N-limited (Cui et al., 2022). Therefore, salinization-induced higher C:N ratios could be responsible for the lower carbon mineralization rates in the high-salinity ponds.

The decrease in DOC concentrations with increasing salinity may also explain the lower carbon mineralization rates in the high-salinity ponds (Figures 6a and 8). DOC is derived from the hydrolysis of organic carbon in sediments by carbon-acquiring enzymes released by microorganisms (Moorhead et al., 2012). Previous studies have reported that a significant increase in salinity may reduce carbon-acquiring enzyme activities by destroying molecular stability and protein confirmation states (Servais et al., 2019). Therefore, a decrease in carbon-acquiring enzyme activities may explain the lower DOC concentrations in the high-salinity ponds. Moreover, increased salinity can decrease the solubility of organic carbon (Tully et al., 2019). This occurs because the increase in salinity can induce cation (e.g., Ca^{2+}) bridging between cations and DOC, which creates flocculent organic matter and reduces DOC concentrations (Adusei-Gyamfi et al., 2019; Decho & Gutierrez, 2017). However, this effect may be limited in the current study because our saline pond sediments were always immersed in saline waters. Thus, the solubility of sediment organic carbon between low-salinity and high-salinity ponds might not be significantly different.

4.4. Microbial Fe(III) Reduction in Ponds With Different Salinities

Consistent with Hypothesis I, the contribution of Fe(III) reduction in the low-salinity ponds (61.1%) was higher than that in the high-salinity ponds (31.1%) (Figure 3). Moreover, the abundance of *Geobacter* significantly decreased from the low-salinity ponds to high-salinity ponds (Figure 4a). There are three probable explanations for the decreasing microbial Fe(III) reduction rates with increasing salinity.

First, sulfate reduction should account for the most important contribution to the decline in microbial Fe(III) reduction as salinity increased (Figures 7 and 8). Higher sulfate reduction rates were observed in the high-salinity ponds compared with the low-salinity ponds (Figure 2b). Although microbial Fe(III) reduction is more energetically favorable than sulfate reduction, the solid phase of Fe(III) greatly limits the competitiveness of Fe(III) reduction (Zhou et al., 2017). This is because iron reducers should attach to the surface of Fe(III) (hydro)oxides to transfer electron acceptors, whereas it is much easier for sulfate reducers to access liquid sulfate (Hyun et al., 2013). Therefore, the intense competition for sulfate reduction should primarily explain the lower microbial Fe(III) reduction rates in high-salinity ponds. Second, abiotic Fe(III) reduction may also be responsible for the decreasing microbial Fe(III) reduction rates in the higher salinity ponds. When the salinity increased, the product of sulfate reduction, that is, $\sum\text{H}_2\text{S}$, accumulated (Burton et al., 2008). Fe(III) could be abiotically reduced by $\sum\text{H}_2\text{S}$ and yield FeS (Mohatt et al., 2011; Sheng et al., 2015). This abiotic Fe(III) reduction has larger reaction kinetics than microbial Fe(III) reduction and thus could compete for Fe(III) with microbial Fe(III) reduction (Kappler et al., 2021; Luo et al., 2015). We observed FeS accumulation with increasing salinity which was negatively related to the microbial Fe(III) reduction rates (Figure 7). This result suggests that the accumulation of FeS is also responsible for the decreasing rates of microbial Fe(III) reduction with the increasing salinity. Third, oxidation-reduction potential may be responsible for the lower microbial Fe(III) reduction rates as salinity increases. In the current study, we found that the sediment ORP was lower in the high-salinity ponds compared with the low-salinity ponds (Table 2). This was probably because higher TOC content in the high-salinity ponds (Table 2) leads to more depletion of electron acceptors and a more reduced environment than in low-salinity ponds (Alongi et al., 1999). Iron reducers prefer a sub-oxic than anaerobic environment (Canfield et al., 1993). Therefore, lower sediment ORP led to lower Fe(III) reduction rates in the high-salinity ponds than low-salinity ponds (Figure 4a).

Overall, the inhibition of sulfate reduction, abiotic Fe(III) reduction, and lower oxidation-reduction potential were all responsible for the decreased rates of microbial Fe(III) reduction in the high-salinity ponds.

4.5. Partitioning of the Carbon Mineralization Pathway in Aquaculture Pond Sediments

To the best of our knowledge, few studies have quantified the partitioning of carbon mineralization pathways in coastal earthen aquaculture pond sediments. Our work highlighted that microbial Fe(III) reduction dominated ($46.1\% \pm 19.1\%$) carbon mineralization in aquaculture pond sediments (Figure 3). These Fe(III) reduction

Table 4

Comparison of the Rates and Contributions of Microbial Fe(III) Reduction in Aquaculture Pond Sediments and Other Aquatic Sediments

Site	Habitat	Depth (cm)	Salinity (mg g ⁻¹)	Rates (μmol g ⁻¹ d ⁻¹)		Contribution (%)	Reference
				Fe(III) reduction	Carbon mineralization		
Alabama, USA	Freshwater wetland	0–3	0	0.36	1.59	23	Roden & Wetzel, 2002
Patuxent River, USA	Freshwater wetland	0–30	0.03	0.00–2.30	2.2–7.80	0–29	Keller et al., 2013
Min River Estuary, China	Saltmarsh	0–10	2–5	0.17–0.60	0.70–1.20	20–89	Luo et al., 2020
Han River Estuary, Korea	Saltmarsh	0–10	13–27	1.00–2.11	1.52–5.85	36–66	Hyun et al., 2009
Skidaway Island, Georgia	Saltmarsh	0–20	20–33	0.43–0.94	1.28–1.63	28–54	Gribsholt et al., 2003
Patuxent River, USA	Saltmarsh	0–10	0–15	0.10–5.10	1.00–8.00	50–57	Neubauer et al., 2005
Peninsula of Michigan, USA	Peatland	0–19	7–35	0.00–0.16	0.08–1.41	0–12	Ye et al., 2012
Bangrong, Thailand	Mangrove	0–20	35	0.00–0.10	0.17–1.10	0–39	Kristensen et al., 2000
Ras Dege, Tanzania	Mangrove	0–10	2–45	0.31–0.37	0.57–1.00	38–54	Kristensen et al., 2011
Baltic-North Sea	Seashore	0–10	20–30	0.01–0.29	0.13–0.40	5–25	Jensen et al., 2003
Ubatuba Bay, Brazilian	Seashore	0–20	33–34	0.00–0.24	0.05–0.30	22	Quintana et al., 2015
Skagerrak, Denmark	Continental shelf	0–10	15–25	0.02–0.04	0.50–1.05	10–27	Canfield et al., 1993
Ulleung Basin, East Sea	Continental shelf	0–20	34–35	0.00–0.24	0.00–0.40	20	Hyun et al., 2017
Conception Bay, Canada	Continental shelf	0–10	31–33	0.01–0.03	0.09–0.16	12–29	Thamdrup & Canfield, 1996
Lake Michigan, USA	Lake	2–18	0	0.20	0.50	44	Thomsen et al., 2004
Lake Taihu, China	Lake	0–16	0	0.78–1.11	1.66–2.46	32–66	Chen & Jiang, 2016
Minjiang and Mulanxi Estuaries, China	Aquaculture pond	0–10	2–16	0.24–1.52	1.02–2.17	46.1 ± 19.1	This study

contributions were higher than those previously reported in continental shelf and seashore sediments (Canfield et al., 1993; Hyun et al., 2017; Jensen et al., 2003; Quintana et al., 2015; Thamdrup & Canfield, 1996), peatland (Ye et al., 2012), and tidal freshwater wetland sediments (Keller et al., 2013; Roden & Wetzel, 2002), and comparable to those reported in saltmarsh sediments (Gribsholt et al., 2003; Hyun et al., 2009; Luo et al., 2020; Neubauer et al., 2005), mangrove sediments (Kristensen et al., 2000, 2011) and lake sediments (Chen & Jiang, 2016; Thomsen et al., 2004), indicating that aquaculture pond sediments are also “hotspots” for microbial Fe(III) reduction (Table 4).

Sulfate reduction also contributed to carbon mineralization (39.6% ± 16.8%). The presence of FeS (Table 2) and high abundance of sulfate reducers (Figure 4b) also implied the high rates of sulfate reduction in aquaculture pond systems. Methanogenesis accounted for <3% of the total carbon mineralization across periods and ponds, indicating a striking suppressive effect of Fe(III) and sulfate reduction on methanogenesis (Roden & Wetzel, 1996). “Unexplained pathways” account for 6.5%–20.1% of the carbon mineralization in the aquaculture pond sediments (Figure 3). There are two possible explanations for this inconsistency. First, the different methodologies adopted for determining the rates of each microbial metabolic pathway can yield errors (von Kamp et al., 2017). Second, other carbon mineralization pathways (e.g., such as denitrification) may contribute to the unexplained pathways (Kim et al., 2015). However, a previous study reported that denitrification accounted for <1% of carbon mineralization in the shrimp aquaculture ponds of the Mekong Delta, Vietnam, owing to limited nitrate concentrations (Alongi et al., 1999). In this study, nitrate concentrations ranged from 0.51 to 2.33 μmol L⁻¹, which was much lower than the sulfate concentrations (2.49–16.03 mmol L⁻¹) (Table 2). Therefore, the contribution of denitrification may be limited in the current study. Nevertheless, additional studies are necessary to explain this missing carbon in aquaculture pond systems.

4.6. Limitation and Uncertainty

The current study experienced a limitation. We applied anaerobic incubation to determine the rates of microbial Fe(III) and sulfate reduction and methanogenesis in the current study. However, the aerators were operational for 2–4 hr daily during farming, leading to a relatively oxic environment in the surface sediment. During this period,

the activity of iron and sulfate reducers and methanogens in the surface sediment may be suppressed. When the aerator was shut down, the aquaculture pond sediments rapidly became anaerobic because the surface sediments were rich in organic matter, and oxygen was utilized rapidly (Alongi et al., 1999). Our sediment ORP data also showed that the sediments were anaerobic when the aerator was not operational (Table 2). Consequently, owing to the oxidation, our experimental protocol may have led to an overestimation of the in situ rates of Fe(III) reduction, sulfate reduction, and methanogenesis during farming.

5. Conclusion

In this study, we reported that microbial Fe(III) reduction played a crucial role in carbon mineralization in the sediments of coastal earthen aquaculture shrimp ponds. Our results also highlight that the rates of microbial Fe(III) reduction vary spatially and temporally in aquaculture shrimp pond systems. Across the three aquaculture farming stages, microbial Fe(III) reduction significantly increased during farming owing to the replenishment of Fe(III). Between the high- and low-salinity ponds, microbial Fe(III) reduction rates decreased as salinity increased owing to the suppression of microbial sulfate reduction, abiotic Fe(III) reduction with sulfides, and lower sediment oxidation-reduction potential. Future models predicting carbon fluxes in aquaculture shrimp pond systems should consider the dynamics of microbial Fe(III) reduction.

Conflict of Interest

The authors declare no conflicts of interest relevant to this study.

Data Availability Statement

Data are deposited in Figshare: <https://figshare.com/s/af124dc35896cc3bbaec>.

Acknowledgments

This work was financially supported by grants from the National Science Foundation of China (32071598; 42077025), the Natural Science Foundation of Fujian Province (2020J01503), the Science and Technology Projects of the Forest Bureau of Fujian Province (2021FKJ30), and Youth Innovation Promotion Association, CAS (2021213).

References

- Adusei-Gyamfi, J., Ouddane, B., Rietveld, L., Cornard, J. P., & Criquet, J. (2019). Natural organic matter-cations complexation and its impact on water treatment: A critical review. *Water Research*, *160*, 130–147. <https://doi.org/10.1016/j.watres.2019.05.064>
- Ali, G., Ling, Z., Saif, I., Usman, M., Jalalah, M., Harraz, F. A., et al. (2021). Biomethanation and microbial community response during agricultural biomass and shrimp chaff digestion. *Environmental Pollution*, *278*, 116801. <https://doi.org/10.1016/j.envpol.2021.116801>
- Alongi, D. M., Tirendi, F., & Trott, L. A. (1999). Rates and pathways of benthic mineralization in extensive shrimp ponds of the Mekong delta, Vietnam. *Aquaculture*, *175*(3–4), 269–292. [https://doi.org/10.1016/S0044-8486\(99\)00077-0](https://doi.org/10.1016/S0044-8486(99)00077-0)
- APHA. (2005). *Standard methods for the examination of water and wastewater* (pp. 3576–3578). American Public Health Association (APHA).
- Beardsley, C., Moss, S., Malfatti, F., & Azam, F. (2011). Quantitative role of shrimp fecal bacteria in organic matter fluxes in a recirculating shrimp aquaculture system. *FEMS Microbiology Ecology*, *77*(1), 134–145. <https://doi.org/10.1111/j.1574-6941.2011.01094.x>
- Bertora, C., Cucu, M. A., Lerda, C., Peyron, M., Bardi, L., Gorra, R., et al. (2018). Dissolved organic carbon cycling, methane emissions and related microbial populations in temperate rice paddies with contrasting straw and water management. *Agriculture, Ecosystems & Environment*, *265*, 292–306. <https://doi.org/10.1016/j.agee.2018.06.004>
- Brodersen, K. E., Trevathan-Tackett, S. M., Nielsen, D. A., Connolly, R. M., Lovelock, C. E., Atwood, T. B., & Macreadie, P. I. (2019). Oxygen consumption and sulfate reduction in vegetated coastal habitats: Effects of physical disturbance. *Frontiers in Marine Science*, *6*, 14. <https://doi.org/10.3389/fmars.2019.00014>
- Burkholder, J. M., & Shumway, S. E. (2011). Bivalve shellfish aquaculture and eutrophication. In *Shellfish aquaculture and the environment* (pp. 155–215). John Wiley & Sons. <https://doi.org/10.1002/9780470960967.ch7>
- Burton, E. D., Sullivan, L. A., Bush, R. T., Johnston, S. G., & Keene, A. F. (2008). A simple and inexpensive chromium-reducible sulfur method for acid-sulfate soils. *Applied Geochemistry*, *23*(9), 2759–2766. <https://doi.org/10.1016/j.apgeochem.2008.07.007>
- Canfield, D. E., Jørgensen, B. B., Fossing, H., Glud, R., Gundersen, J., Ramsing, N. B., et al. (1993). Pathways of organic carbon oxidation in three continental margin sediments. *Marine Geology*, *113*(1–2), 27–40. [https://doi.org/10.1016/0025-3227\(93\)90147-N](https://doi.org/10.1016/0025-3227(93)90147-N)
- Chanda, A., Das, S., Bhattacharyya, S., Das, I., Giri, S., Mukhopadhyay, A., et al. (2019). CO₂ fluxes from aquaculture ponds of a tropical wetland: Potential of multiple lime treatment in reduction of CO₂ emission. *Science of the Total Environment*, *655*, 1321–1333. <https://doi.org/10.1016/j.scitotenv.2018.11.332>
- Chen, C., Hall, S. J., Coward, E., & Thompson, A. (2020). Iron-mediated organic matter decomposition in humid soils can counteract protection. *Nature Communications*, *11*(1), 1–13. <https://doi.org/10.1038/s41467-020-16071-5>
- Chen, M., & Jiang, H. L. (2016). Relative contribution of iron reduction to sediments organic matter mineralization in contrasting habitats of a shallow eutrophic freshwater lake. *Environmental Pollution*, *213*, 904–912. <https://doi.org/10.1016/j.envpol.2016.03.061>
- Chen, X., Miao, W., Yang, Y., Hao, S., & Mao, S. (2020). Aeration-assisted sulfite activation with ferrous for enhanced chloramphenicol degradation. *Chemosphere*, *238*, 124599. <https://doi.org/10.1016/j.chemosphere.2019.124599>
- Chen, Y., Dong, S., Wang, Z., Wang, F., Gao, Q., Tian, X., & Xiong, Y. (2015). Variations in CO₂ fluxes from grass carp *Ctenopharyngodon idella* aquaculture polyculture ponds. *Aquaculture Environment Interactions*, *8*, 31–40. <https://doi.org/10.3354/aei00149>
- Cline, J. D. (1969). Spectrophotometric determination of hydrogen sulfide in natural waters. *Limnology & Oceanography*, *14*(3), 454–458. <https://doi.org/10.4319/lo.1969.14.3.0454>

- Coble, P. G., Del Castillo, C. E., & Avril, B. (1998). Distribution and optical properties of CDOM in the Arabian Sea during the 1995 Southwest Monsoon. *Deep Sea Research Part II: Topical Studies in Oceanography*, 45(10–11), 2195–2223. [https://doi.org/10.1016/S0967-0645\(98\)00068-X](https://doi.org/10.1016/S0967-0645(98)00068-X)
- Cui, J., Zhu, R., Wang, X., Xu, X., Ai, C., He, P., et al. (2022). Effect of high soil C/N ratio and nitrogen limitation caused by the long-term combined organic-inorganic fertilization on the soil microbial community structure and its dominated SOC decomposition. *Journal of Environmental Management*, 303, 114155. <https://doi.org/10.1016/j.jenvman.2021.114155>
- Dawood, M. A., Koshio, S., & Esteban, M. Á. (2018). Beneficial roles of feed additives as immunostimulants in aquaculture: A review. *Reviews in Aquaculture*, 10(4), 950–974. <https://doi.org/10.1111/raq.12209>
- Decho, A. W., & Gutierrez, T. (2017). Microbial extracellular polymeric substances (EPSs) in ocean systems. *Frontiers in Microbiology*, 8, 922. <https://doi.org/10.3389/fmicb.2017.00922>
- de Melo, M. L., Kothawala, D. N., Bertilsson, S., Amaral, J. H., Forsberg, B., & Sarmiento, H. (2020). Linking dissolved organic matter composition and bacterioplankton communities in an Amazon floodplain system. *Limnology & Oceanography*, 65(1), 63–76. <https://doi.org/10.1002/lno.11250>
- Ding, L. J., Su, J. Q., Xu, H. J., Jia, Z. J., & Zhu, Y. G. (2015). Long-term nitrogen fertilization of paddy soil shifts iron-reducing microbial community revealed by RNA-¹³C-acetate probing coupled with pyrosequencing. *The ISME Journal*, 9(3), 721–734. <https://doi.org/10.1038/ismej.2014.159>
- Dombrowski, N., Teske, A. P., & Baker, B. J. (2018). Expansive microbial metabolic versatility and biodiversity in dynamic Guaymas Basin hydrothermal sediments. *Nature Communications*, 9(1), 1–13. <https://doi.org/10.1038/s41467-018-07418-0>
- Emmerich, M., Bhansali, A., Lösekann-Behrens, T., Schröder, C., Kappler, A., & Behrens, S. (2012). Abundance, distribution, and activity of Fe (II)-oxidizing and Fe (III)-reducing microorganisms in hypersaline sediments of Lake Kasin, southern Russia. *Applied and Environmental Microbiology*, 78(12), 4386–4399. <https://doi.org/10.1128/AEM.07637-11>
- FAO. (2014). *The state of world fisheries and aquaculture 2014: Opportunities and challenges*. Food and Agriculture Organization of the United Nations (FAO).
- FAO. (2016). *The state of world fisheries and aquaculture 2016: Contributing to food security and nutrition for all*. Food and Agriculture Organization of the United Nations (FAO).
- Froelich, P., Klinkhammer, G. P., Bender, M. L., Luedtke, N. A., Heath, G. R., Cullen, D., et al. (1979). Early oxidation of organic matter in pelagic sediments of the eastern equatorial Atlantic: Suboxic diagenesis. *Geochimica et Cosmochimica Acta*, 43(7), 1075–1090. [https://doi.org/10.1016/0016-7037\(79\)90095-4](https://doi.org/10.1016/0016-7037(79)90095-4)
- Graeber, D., Gelbrecht, J., Pusch, M. T., Anlanger, C., & von Schiller, D. (2012). Agriculture has changed the amount and composition of dissolved organic matter in Central European headwater streams. *Science of the Total Environment*, 438, 435–446. <https://doi.org/10.1016/j.scitotenv.2012.08.087>
- Gribsholt, B., Kostka, J. E., & Kristensen, E. (2003). Impact of fiddler crabs and plant roots on sediment biogeochemistry in a Georgia saltmarsh. *Marine Ecology Progress Series*, 259, 237–251. <https://doi.org/10.3354/meps259237>
- Herbert, E. R., Boon, P., Burgin, A. J., Neubauer, S. C., Franklin, R. B., Ardón, M., et al. (2015). A global perspective on wetland salinization: Ecological consequences of a growing threat to freshwater wetlands. *Ecosphere*, 6(10), 1–43. <https://doi.org/10.1890/ES14-00534.1>
- Holgerson, M. A. (2015). Drivers of carbon dioxide and methane supersaturation in small, temporary ponds. *Biogeochemistry*, 124(1), 305–318. <https://doi.org/10.1007/s10533-015-0099-y>
- Holgerson, M. A., & Raymond, P. A. (2016). Large contribution to inland water CO₂ and CH₄ emissions from very small ponds. *Nature Geoscience*, 9(3), 222–226. <https://doi.org/10.1038/ngeo2654>
- Holmes, D. E., Finneran, K. T., O'neil, R. A., & Lovley, D. R. (2002). Enrichment of members of the family *Geobacteraceae* associated with stimulation of dissimilatory metal reduction in uranium-contaminated aquifer sediments. *Applied and Environmental Microbiology*, 68(5), 2300–2306. <https://doi.org/10.1128/aem.68.5.2300-2306.2002>
- Hou, L., Zheng, Y., Liu, M., Gong, J., Zhang, X., Yin, G., & You, L. (2013). Anaerobic ammonium oxidation (anammox) bacterial diversity, abundance, and activity in marsh sediments of the Yangtze Estuary. *Journal of Geophysical Research: Biogeosciences*, 118(3), 1237–1246. <https://doi.org/10.1002/jgrg.20108>
- Hyun, J. H., Kim, S. H., Mok, J. S., Cho, H., Lee, T., Vandieken, V., & Thamdrup, B. (2017). Manganese and iron reduction dominate organic carbon oxidation in surface sediments of the deep Ulleung Basin, East Sea. *Biogeosciences*, 14(4), 941–958. <https://doi.org/10.1016/j.marpolbul.2013.07.004>
- Hyun, J. H., Kim, S. H., Mok, J. S., Lee, J. S., An, S. U., Lee, W. C., & Jung, R. H. (2013). Impacts of long-line aquaculture of Pacific oysters (*Crassostrea gigas*) on sulfate reduction and diffusive nutrient flux in the coastal sediments of Jinhae-Tongyeong, Korea. *Marine Pollution Bulletin*, 74(1), 187–198. <https://doi.org/10.1016/j.marpolbul.2013.07.004>
- Hyun, J. H., Mok, J. S., Cho, H. Y., Kim, S. H., Lee, K. S., & Kostka, J. E. (2009). Rapid organic matter mineralization coupled to iron cycling in intertidal mud flats of the Han River estuary, Yellow Sea. *Biogeochemistry*, 92(3), 231–245. <https://doi.org/10.1007/s10533-009-9287-y>
- Jensen, M. M., Thamdrup, B., Rysgaard, S., Holmer, M., & Fossing, H. (2003). Rates and regulation of microbial iron reduction in sediments of the Baltic-North Sea transition. *Biogeochemistry*, 65(3), 295–317. <https://doi.org/10.1023/A:1026261303494>
- Johnston, S. G., Keene, A. F., Bush, R. T., Burton, E. D., Sullivan, L. A., Isaacson, L., et al. (2011). Iron geochemical zonation in a tidally inundated acid sulfate soil wetland. *Chemical Geology*, 280(3–4), 257–270. <https://doi.org/10.1016/j.chemgeo.2010.11.014>
- Kappler, A., Bryce, C., Mansor, M., Lueder, U., Byrne, J. M., & Swanner, E. D. (2021). An evolving view on biogeochemical cycling of iron. *Nature Reviews Microbiology*, 19(6), 360–374. <https://doi.org/10.1038/s41579-020-00502-7>
- Keller, J. K., Sutton-Grier, A. E., Bullock, A. L., & Megonigal, J. P. (2013). Anaerobic metabolism in tidal freshwater wetlands: I. Plant removal effects on iron reduction and methanogenesis. *Estuaries and Coasts*, 36(3), 457–470. <https://doi.org/10.1007/s12237-012-9527-6>
- Khan, I., Fahad, S., Wu, L., Zhou, W., Xu, P., Sun, Z., et al. (2019). Labile organic matter intensifies phosphorus mobilization in paddy soils by microbial iron(III) reduction. *Geoderma*, 352, 185–196. <https://doi.org/10.1016/j.geoderma.2019.06.011>
- Kim, S. H., An, S. U., Lee, W. C., Lee, J. S., & Hyun, J. H. (2020). Influence of Manila clam aquaculture on rates and partitioning of organic carbon oxidation in sediment of Keunso Bay, Yellow Sea. *Aquaculture Environment Interactions*, 12, 91–103. <https://doi.org/10.3354/aei00352>
- Kim, S. Y., Veraart, A. J., Meima-Franke, M., & Bodelier, P. L. (2015). Combined effects of carbon, nitrogen and phosphorus on CH₄ production and denitrification in wetland sediments. *Geoderma*, 259, 354–361. <https://doi.org/10.1016/j.geoderma.2015.03.015>
- Kostka, J. E., & Luther, G. W., III. (1994). Partitioning and speciation of solid phase iron in saltmarsh sediments. *Geochimica et Cosmochimica Acta*, 58(7), 1701–1710. [https://doi.org/10.1016/0016-7037\(94\)90531-2](https://doi.org/10.1016/0016-7037(94)90531-2)
- Kostka, J. E., Roychoudhury, A., & Van Cappellen, P. (2002). Rates and controls of anaerobic microbial respiration across spatial and temporal gradients in saltmarsh sediments. *Biogeochemistry*, 60(1), 49–76. <https://doi.org/10.1023/A:1016525216426>

- Kristensen, E., Andersen, F. Ø., Holmboe, N., Holmer, M., & Thongtham, N. (2000). Carbon and nitrogen mineralization in sediments of the Bangrong mangrove area, Phuket, Thailand. *Aquatic Microbial Ecology*, 22(2), 199–213. <https://doi.org/10.3354/ame022199>
- Kristensen, E., Mangion, P., Tang, M., Flindt, M. R., Holmer, M., & Ulomi, S. (2011). Microbial carbon oxidation rates and pathways in sediments of two Tanzanian mangrove forests. *Biogeochemistry*, 103(1), 143–158. <https://doi.org/10.1007/s10533-010-9453-2>
- Lai, J., Zou, Y., Zhang, J., & Peres-Neto, P. R. (2022). Generalizing hierarchical and variation partitioning in multiple regression and canonical analyses using the rdacca.hp R package. *Methods in Ecology and Evolution*, 13(4), 782–788. <https://doi.org/10.1111/2041-210x.13800>
- Lamers, L. P., Van Diggelen, J. M., Op den Camp, H. J., Visser, E. J., Lucassen, E. C., Vile, M. A., et al. (2012). Microbial transformations of nitrogen, sulfur, and iron dictate vegetation composition in wetlands: A review. *Frontiers in Microbiology*, 3, 156. <https://doi.org/10.3389/fmicb.2012.00156>
- Lawaetz, A. J., & Stedmon, C. A. (2009). Fluorescence intensity calibration using the Raman scatter peak of water. *Applied Spectroscopy*, 63(8), 936–940. <https://doi.org/10.1366/000370209788964548>
- Lemonnier, H., Royer, F., Caradec, F., Lopez, E., Hubert, C., Rabiller, É., et al. (2021). Diagenetic processes in aquaculture ponds showing metal accumulation on shrimp gills. *Frontiers in Marine Science*, 8, 625789. <https://doi.org/10.3389/fmars.2021.625789>
- Li, H., Peng, J., Weber, K. A., & Zhu, Y. (2011). Phylogenetic diversity of Fe(III)-reducing microorganisms in rice paddy soil: Enrichment cultures with different short-chain fatty acids as electron donors. *Journal of Soils and Sediments*, 11(7), 1234–1242. <https://doi.org/10.1007/s11368-011-0371-2>
- Liu, Y., Luo, M., Ye, R., Huang, J., Xiao, L., Hu, Q., et al. (2019). Impacts of the rhizosphere effect and plant species on organic carbon mineralization rates and pathways, and bacterial community composition in a tidal marsh. *FEMS Microbiology Ecology*, 95(9), fiz120. <https://doi.org/10.1093/femsec/fiz120>
- Lukawska-Matuszewska, K., Graca, B., Broclawik, O., & Zalewska, T. (2019). The impact of declining oxygen conditions on pyrite accumulation in shelf sediments (Baltic Sea). *Biogeochemistry*, 142(2), 209–230. <https://doi.org/10.1007/s10533-018-0530-2>
- Luo, M., Zeng, C. S., Tong, C., Huang, J. F., Chen, K., & Liu, F. Q. (2016). Iron reduction along an inundation gradient in a tidal sedge (*Cyperus malaccensis*) marsh: The rates, pathways, and contributions to anaerobic organic matter mineralization. *Estuaries and Coasts*, 39(6), 1679–1693. <https://doi.org/10.1007/s12237-016-0094-0>
- Luo, M., Zeng, C. S., Tong, C., Huang, J. F., Yu, Q., Guo, Y. B., & Wang, S. H. (2014). Abundance and speciation of iron across a subtropical tidal marsh of the Min River Estuary in the East China Sea. *Applied Geochemistry*, 45, 1–13. <https://doi.org/10.1016/j.apgeochem.2014.02.014>
- Luo, M., Zeng, C. S., Tong, C., Huang, J. F., Yu, Q., Guo, Y. B., & Wang, S. H. (2015). Kinetics of chemical and microbial iron reduction along an inundation gradient in a tidal marsh of the Min River Estuary, southeastern China. *Geomicrobiology Journal*, 32(7), 635–647. <https://doi.org/10.1080/01490451.2014.950362>
- Luo, M., Zhai, Z., Ye, R., Xing, R., Huang, J., & Tong, C. (2020). Carbon mineralization in tidal freshwater marsh soils at the intersection of low-level saltwater intrusion and ferric iron loading. *Catena*, 193, 104644. <https://doi.org/10.1016/j.catena.2020.104644>
- Luo, M., Zhu, W., Huang, J., Liu, Y., Duan, X., Wu, J., & Tong, C. (2019). Anaerobic organic carbon mineralization in tidal wetlands along a low-level salinity gradient of a subtropical estuary: Rates, pathways, and controls. *Geoderma*, 337, 1245–1257. <https://doi.org/10.1016/j.geoderma.2018.07.030>
- Ma, Y., Sun, L., Liu, C., Yang, X., Zhou, W., Yang, B., et al. (2018). A comparison of methane and nitrous oxide emissions from inland mixed-fish and crab aquaculture ponds. *Science of the Total Environment*, 637, 517–523. <https://doi.org/10.1016/j.scitotenv.2018.05.040>
- Millero, F. J. (2010). History of the equation of state of seawater. *Oceanography*, 23(3), 18–33. <https://doi.org/10.5670/oceanog.2010.21>
- Millero, F. J., Feistel, R., Wright, D. G., & McDougall, T. J. (2008). The composition of standard seawater and the definition of the Reference-Composition Salinity Scale. *Deep Sea Research I*, 55(1), 50–72. <https://doi.org/10.1016/j.dsr.2007.10.001>
- Mohatt, J. L., Hu, L., Finneran, K. T., & Strathmann, T. J. (2011). Microbially mediated abiotic transformation of the antimicrobial agent sulfamethoxazole under iron-reducing soil conditions. *Environmental Science & Technology*, 45(11), 4793–4801. <https://doi.org/10.1021/es200413g>
- Mok, J. S., Choi, A., Kim, B., An, S. U., Lee, W. C., Kim, H. C., et al. (2021). Phosphorus dynamics associated with organic carbon mineralization by reduction of sulfate and iron in sediment exposed to fish farming. *Frontiers in Marine Science*, 8, 645449. <https://doi.org/10.3389/fmars.2021.645449>
- Moorhead, D. L., Lashermes, G., & Sinsabaugh, R. L. (2012). A theoretical model of C- and N-acquiring exoenzyme activities, which balances microbial demands during decomposition. *Soil Biology and Biochemistry*, 53, 133–141. <https://doi.org/10.1016/j.soilbio.2012.05.011>
- Mulat, D. G., Jacobi, H. F., Feilberg, A., Adamsen, A. P. S., Richnow, H. H., & Nikolausz, M. (2016). Changing feeding regimes to demonstrate flexible biogas production: Effects on process performance, microbial community structure, and methanogenesis pathways. *Applied and Environmental Microbiology*, 82(2), 438–449. <https://doi.org/10.1128/AEM.02320-15>
- Murphy, K. R., Hambly, A., Singh, S., Henderson, R. K., Baker, A., Stuetz, R., & Khan, S. J. (2011). Organic matter fluorescence in municipal water recycling schemes: Toward a unified PARAFAC model. *Environmental Science & Technology*, 45(7), 2909–2916. <https://doi.org/10.1021/es103015e>
- Naylor, R. L., Hardy, R. W., Buschmann, A. H., Bush, S. R., Cao, L., Klinger, D. H., et al. (2021). A 20-year retrospective review of global aquaculture. *Nature*, 591(7851), 551–563. <https://doi.org/10.1038/s41586-021-03308-6>
- Neubauer, S. C., Givler, K., Valentine, S., & Megonigal, J. P. (2005). Seasonal patterns and plant-mediated controls of subsurface wetland biogeochemistry. *Ecology*, 86(12), 3334–3344. <https://doi.org/10.1890/04-1951>
- Nho, S. W., Abdelhamed, H., Paul, D., Park, S., Muel, M. J., Karsi, A., & Lawrence, M. L. (2018). Taxonomic and functional metagenomic profile of sediment from a commercial catfish pond in Mississippi. *Frontiers in Microbiology*, 9, 2855. <https://doi.org/10.3389/fmicb.2018.02855>
- Oksanen, J., Kindt, R., Legendre, P., O'Hara, B., Stevens, M. H. H., Oksanen, M. J., & Suggests, M. A. S. S. (2007). The vegan package. *Community Ecology Package*, 10(631–637), 719.
- Pereyra, L. P., Hiibel, S. R., Prieto Riquelme, M. V., Reardon, K. F., & Pruden, A. (2010). Detection and quantification of functional genes of cellulose-degrading, fermentative, and sulfate-reducing bacteria and methanogenic archaea. *Applied and Environmental Microbiology*, 76(7), 2192–2202. <https://doi.org/10.1128/AEM.01285-09>
- Pusceddu, A., Della Patrona, L., & Beliaeff, B. (2011). Trophic status of earthen ponds used for semi-intensive shrimp (*Litopenaeus stylirostris*, Stimpson, 1874) farming in New Caledonia (Pacific Ocean). *Marine Environmental Research*, 72(4), 160–171. <https://doi.org/10.1016/j.marenvres.2011.07.005>
- Quintana, C. O., Shimabukuro, M., Pereira, C. O., Alves, B. G., Moraes, P. C., Valdemarsen, T., et al. (2015). Carbon mineralization pathways and bioturbation in coastal Brazilian sediments. *Scientific Reports*, 5(1), 1–13. <https://doi.org/10.1038/srep16122>
- R Core Team. (2013). R: A Language and Environment for Statistical Computing. R Foundation for Statistical Computing.

- Redmile-Gordon, M. A., Evershed, R. P., Hirsch, P. R., White, R. P., & Goulding, K. (2015). Soil organic matter and the extracellular microbial matrix show contrasting responses to C and N availability. *Soil Biology and Biochemistry*, 88, 257–267. <https://doi.org/10.1016/j.soilbio.2015.05.025>
- Reis, J., Weldon, A., Ito, P., Stites, W., Rhodes, M., & Davis, D. A. (2021). Automated feeding systems for shrimp: Effects of feeding schedules and passive feedback feeding systems. *Aquaculture*, 541, 736800. <https://doi.org/10.1016/j.aquaculture.2021.736800>
- Roden, E. E., & Wetzel, R. G. (1996). Organic carbon oxidation and suppression of methane production by microbial Fe(III) oxide reduction in vegetated and unvegetated freshwater wetland sediments. *Limnology & Oceanography*, 41(8), 1733–1748. <https://doi.org/10.4319/lo.1996.41.8.1733>
- Roden, E. E., & Wetzel, R. G. (2002). Kinetics of microbial Fe (III) oxide reduction in freshwater wetland sediments. *Limnology & Oceanography*, 47(1), 198–211. <https://doi.org/10.4319/lo.2002.47.1.0198>
- Rosseel, Y. (2012). lavaan: An R package for structural equation modeling. *Journal of Statistical Software*, 48(2), 1–36. <https://doi.org/10.18637/jss.v048.i02>
- Sabu, E. A., Gonsalves, M. J., Nazareth, D., & Sreepada, R. A. (2022). Influence of environmental variables on methane related microbial activities in a tropical bio-secured zero-exchange shrimp culture system. *Aquaculture Reports*, 22, 100950. <https://doi.org/10.1016/j.aqrep.2021.100950>
- Schoepfer, V. A., Bernhardt, E. S., & BurginIron, A. J. (2014). Iron clad wetlands: Soil iron-sulfur buffering determines coastal wetland response to salt water incursion. *Journal of Geophysical Research: Biogeosciences*, 119(12), 2209–2219. <https://doi.org/10.1002/2014JG002739>
- Servais, S., Kominoski, J. S., Charles, S. P., Gaiser, E. E., Mazzei, V., Troxler, T. G., & Wilson, B. J. (2019). Saltwater intrusion and soil carbon loss: Testing effects of salinity and phosphorus loading on microbial functions in experimental freshwater wetlands. *Geoderma*, 337, 1291–1300. <https://doi.org/10.1016/j.geoderma.2018.11.013>
- Sheng, Y., Sun, Q., Bottrell, S. H., & Mortimer, R. J. G. (2015). Reduced inorganic sulfur and its bioavailability in surface sediment in offshore areas of NE China. *Environmental Science: Processes & Impacts*, 17(9), 1689–1697. <https://doi.org/10.1039/c5em00175g>
- Stainton, M. P. (1973). A syringe gas-stripping procedure for gas-chromatographic determination of dissolved inorganic and organic carbon in fresh water and carbonates in sediments. *Journal of the Fisheries Research Board of Canada*, 30(10), 1441–1445. <https://doi.org/10.1139/f73-234>
- Stams, A. J., De Bok, F. A., Plugge, C. M., Van Eekert, M. H., Dolfig, J., & Schraa, G. (2006). Exocellular electron transfer in anaerobic microbial communities. *Environmental Microbiology*, 8(3), 371–382. <https://doi.org/10.1111/j.1462-2920.2006.00989.x>
- Stedmon, C. A., & Bro, R. (2008). Characterizing dissolved organic matter fluorescence with parallel factor analysis: A tutorial. *Limnology and Oceanography: Methods*, 6(11), 572–579. <https://doi.org/10.4319/lom.2008.6.572>
- Stedmon, C. A., & Markager, S. (2005). Tracing the production and degradation of autochthonous fractions of dissolved organic matter by fluorescence analysis. *Limnology & Oceanography*, 50(5), 1415–1426. <https://doi.org/10.4319/lo.2005.50.5.1415>
- Stedmon, C. A., Markager, S., & Bro, R. (2003). Tracing dissolved organic matter in aquatic environments using a new approach to fluorescence spectroscopy. *Marine Chemistry*, 82(3–4), 239–254. [https://doi.org/10.1016/S0272-7714\(03\)00003-9](https://doi.org/10.1016/S0272-7714(03)00003-9)
- Steinberg, L. M., & Regan, J. M. (2009). *mcrA*-targeted real-time quantitative PCR method to examine methanogen communities. *Applied and Environmental Microbiology*, 75(13), 4435–4442. <https://doi.org/10.1128/AEM.02858-08>
- Suárez-Abelenda, M., Ferreira, T. O., Camps-Arbestain, M., Rivera-Monroy, V. H., Macías, F., Nóbrega, G. N., & Otero, X. (2014). The effect of nutrient-rich effluents from shrimp farming on mangrove soil carbon storage and geochemistry under semi-arid climate conditions in northern Brazil. *Geoderma*, 213, 551–559. <https://doi.org/10.1016/j.geoderma.2013.08.007>
- Thamdrup, B. O., & Canfield, D. E. (1996). Pathways of carbon oxidation in continental margin sediments off central Chile. *Limnology & Oceanography*, 41(8), 1629–1650. <https://doi.org/10.4319/lo.1996.41.8.1629>
- Tho, N., Ut, V. N., & Merckx, R. (2011). Physico-chemical characteristics of the improved extensive shrimp farming system in the Mekong Delta of Vietnam. *Aquaculture Research*, 42(11), 1600–1614. <https://doi.org/10.1111/j.1365-2109.2010.02750.x>
- Thomsen, U., Thamdrup, B., Stahl, D. A., & Canfield, D. E. (2004). Pathways of organic carbon oxidation in a deep lacustrine sediment, Lake Michigan. *Limnology & Oceanography*, 49(6), 2046–2057. <https://doi.org/10.4319/lo.2004.49.6.2046>
- Tong, C., Bastviken, D., Tang, K. W., Yang, P., Yang, H., Zhang, Y., et al. (2021). Annual CO₂ and CH₄ fluxes in coastal earthen ponds with *Litopenaeus vannamei* in southeastern China. *Aquaculture*, 545, 737229. <https://doi.org/10.1016/j.aquaculture.2021.737229>
- Tong, Y., Wang, X., Sun, Z., & Gao, J. (2021). Two transformation pathways of acetaminophen with Fe³⁺ saturated clay particles in dark or light. *Chemosphere*, 278, 130399. <https://doi.org/10.1016/j.chemosphere.2021.130399>
- Tully, K. L., Weissman, D., Wyner, W. J., Miller, J., & Jordan, T. (2019). Soils in transition: Saltwater intrusion alters soil chemistry in agricultural fields. *Biogeochemistry*, 142(3), 339–356. <https://doi.org/10.1007/s10533-019-00538-9>
- Vermeire, M. L., Bonneville, S., Stenuit, B., Delvaux, B., & Cornélis, J. T. (2019). Is microbial reduction of Fe(III) in podzolic soils influencing C release. *Geoderma*, 340, 1–10. <https://doi.org/10.1016/j.geoderma.2018.12.045>
- von Kamp, A., Thiele, S., Hädicke, O., & Klant, S. (2017). Use of *CellNetAnalyzer* in biotechnology and metabolic engineering. *Journal of Biotechnology*, 261, 221–228. <https://doi.org/10.1016/j.jbiotec.2017.05.001>
- Wang, K., Jia, R., Li, L., Jiang, R., & Qu, D. (2020). Community structure of *Anaeromyxobacter* in Fe (III) reducing enriched cultures of paddy soils. *Journal of Soils and Sediments*, 20(3), 1621–1631. <https://doi.org/10.1007/s11368-019-02529-7>
- Wang, Y., Ling, J., Gu, C., Zhou, S., & Jin, X. (2021). Dissolution of Fe from Fe-bearing minerals during the brown-carbonization processes in atmosphere. *Science of the Total Environment*, 791, 148133. <https://doi.org/10.1016/j.scitotenv.2021.148133>
- Weston, N. B., Dixon, R. E., & Joye, S. B. (2006). Ramifications of increased salinity in tidal freshwater sediments: Geochemistry and microbial pathways of organic matter mineralization. *Journal of Geophysical Research*, 111(G1), G01009. <https://doi.org/10.1029/2005JG000071>
- Yan, C., Sheng, Y., Ju, M., Ding, C., Li, Q., Luo, Z., et al. (2020). Relationship between the characterization of natural colloids and metal elements in surface waters. *Environmental Science and Pollution Research*, 27(25), 31872–31883. <https://doi.org/10.1007/s11356-020-09500-x>
- Yang, P., Zhang, Y., Lai, D. Y., Tan, L., Jin, B., & Tong, C. (2018). Fluxes of carbon dioxide and methane across the water-atmosphere interface of aquaculture shrimp ponds in two subtropical estuaries: The effect of temperature, substrate, salinity and nitrate. *Science of the Total Environment*, 635, 1025–1035. <https://doi.org/10.1016/j.scitotenv.2018.04.102>
- Ye, R., Jin, Q., Bohannon, B., Keller, J. K., McAllister, S. A., & Bridgman, S. D. (2012). pH controls over anaerobic carbon mineralization, the efficiency of methane production, and methanogenic pathways in peatlands across an ombrotrophic–minerotrophic gradient. *Soil Biology and Biochemistry*, 54, 36–47. <https://doi.org/10.1016/j.soilbio.2012.05.015>
- Yu, R. Q., Flanders, J. R., Mack, E. E., Turner, R., Mirza, M. B., & Barkay, T. (2012). Contribution of coexisting sulfate and iron reducing bacteria to methylmercury production in freshwater river sediments. *Environmental Science & Technology*, 46(5), 2684–2691. <https://doi.org/10.1021/es2033718>
- Yuan, J., Liu, D., Xiang, J., He, T., Kang, H., & Ding, W. (2021). Methane and nitrous oxide have separated production zones and distinct emission pathways in freshwater aquaculture ponds. *Water Research*, 190, 116739. <https://doi.org/10.1016/j.watres.2020.116739>

- Yuan, J., Xiang, J., Liu, D., Kang, H., He, T., Kim, S., et al. (2019). Rapid growth in greenhouse gas emissions from the adoption of industrial-scale aquaculture. *Nature Climate Change*, 9(4), 318–322. <https://doi.org/10.1038/s41558-019-0425-9>
- Zhang, X., Sun, Y., Ma, F., Li, A., & Yang, J. (2020). Role of soluble microbial product as an intermediate electron station linking C/N and nitrogen removal performance in sequencing batch reactor. *Environmental Research*, 183, 109248. <https://doi.org/10.1016/j.envres.2020.109248>
- Zhang, Y., Qin, Z., Li, T., & Zhu, X. (2022). Carbon dioxide uptake overrides methane emission at the air-water interface of algae-shellfish mariculture ponds: Evidence from eddy covariance observations. *Science of the Total Environment*, 815, 152867. <https://doi.org/10.1016/j.scitotenv.2021.152867>
- Zhou, C., Zhou, Y., & Rittmann, B. E. (2017). Reductive precipitation of sulfate and soluble Fe(III) by *Desulfovibrio vulgaris*: Electron donor regulates intracellular electron flow and nano-FeS crystallization. *Water Research*, 119, 91–101. <https://doi.org/10.1016/j.watres.2017.04.044>
- Zhou, R., Hou, D., Zeng, S., Wei, D., Yu, L., Bao, S., et al. (2022). Sedimentary nitrogen and sulfur reduction functional couplings interplay with the microbial community of anthropogenic shrimp culture pond ecosystem. *Frontiers in Microbiology*, 713. <https://doi.org/10.3389/fmicb.2022.830777>